Lithos 107 (2009) 135–151

Contents lists available at ScienceDirect

Lithos

journal homepage: www.elsevier.com/locate/lithos

Geochemical and B–Sr–Nd isotopic evidence for mingling and mixing processes in the magmatic system that fed the Astroni volcano (4.1–3.8 ka) within the Campi Flegrei caldera (southern Italy)

Sonia Tonarini [a,*], Massimo D'Antonio [b,c], Mauro Antonio Di Vito [c], Giovanni Orsi [c], Antonio Carandente [c]

[a] Istituto di Geoscienze e Georisorse, Consiglio Nazionale delle Ricerche, Pisa, Italy
[b] Dipartimento di Scienze della Terra, "University Federico II", Napoli, Italy
[c] Istituto Nazionale di Geofisica e Vulcanologia, Osservatorio Vesuviano, Napoli, Italy

ARTICLE INFO

Article history:
Received 6 June 2008
Accepted 18 September 2008
Available online 21 October 2008

Keywords:
Campi Flegrei caldera
B–Sr–Nd isotope geochemistry
Magma mingling/mixing
Chemostratigraphy

ABSTRACT

The Astroni volcano was built through seven eruptions that generated pyroclastic deposits and lava domes within the Campi Flegrei caldera (southern Italy) 4.1–3.8 ka BP. Whole-rock geochemical and B–Sr–Nd isotopic investigations were carried out on representative samples of all seven eruptions. The products vary from tephriphonolites to phonolites, and from latites to trachytes. They show textural, mineralogical and isotopic evidence of disequilibrium, including distinct clinopyroxene populations, rounded and/or resorbed plagioclase and alkali-feldspar, and reverse-zoned phenocrysts of all these mineral phases. The Sr, Nd and B isotopic composition of whole rocks is variable and correlated with the degree of chemical evolution, suggesting open-system processes in addition to fractional crystallisation. Moreover, significant Sr-isotopic disequilibrium between the phenocrysts and glass has been documented for one sample.

The chemostratigraphy of the products indicates that Astroni eruptions 1 through 5 were fed by magmas of trachytic to phonolitic composition that were less enriched in radiogenic Sr and ^{11}B up-section. This variability has been interpreted as the result of mingling between at least two distinct magmatic end-members, one more evolved and the other less evolved. Another heterogeneous batch of magma, resulting from almost complete mixing between the same two end-members, was drained during eruptions 6 and 7. The more evolved end-member, characterised by $^{87}Sr/^{86}Sr \geq 0.7075$, $^{143}Nd/^{144}Nd \leq 0.51247$ and $\delta^{11}B \geq -8‰$, was very similar to the magma that fed the final phases of the Agnano–Monte Spina eruption, which occurred a few centuries earlier in the Astroni vent area. The less evolved end-member had $^{87}Sr/^{86}Sr \leq 0.70726$, $^{143}Nd/^{144}Nd \geq 0.51251$ and $\delta^{11}B \leq 10‰$, and was likely derived by fractional crystallisation of a mantle-derived magma. An abrupt decrease in both the Sr isotope ratio and the Th content, detected at the transition between Unit 4 and 5, suggests that another magma with a $^{87}Sr/^{86}Sr$ ratio intermediate between those of the two identified end-members may have been involved in Astroni activity. The more evolved end-member is interpreted as a residue of the Agnano–Monte Spina eruption that was invaded by either the intermediate or the less evolved magmatic end-member, promoting mingling and triggering Astroni activity. This study of Astroni provides insights for both short- and long-term volcanic hazard assessment, as the Astroni volcano is the best example of a very close sequence of eruptions from the same vent area in the Campi Flegrei caldera.

1. Introduction

In many volcanoes worldwide igneous rocks exhibit textural, mineralogical and geochemical evidence of having been produced through interaction among distinct magmas. Volcanic rocks resulting from the interaction between either mafic and felsic, or more frequently, differently evolved felsic magmas, have been documented. Examples can be found in intraplate volcanoes and volcanic complexes, such as Black Mountain in south-western Nevada, U.S.A. (e.g., Vogel et al., 1987), Gran Canaria in the Canary Islands (e.g., Troll and Schmincke, 2002), Mt. Etna in southern Italy (e.g., Viccaro et al., 2006), as well as in convergent margin, subduction-related volcanoes and volcanic complexes, such as Arenal volcano in Costa Rica (e.g., Cigolini, 1998), Lassen volcanic center in California, U.S.A. (e.g., Clynne, 1999), Unzen volcano in south-western Japan (e.g., Browne et al., 2006), Stromboli Island (e.g., Cortés et al., 2005) and Mt. Vesuvius in southern Italy (e.g., Civetta et al., 1991b; Santacroce et al., 1993; Cioni et al., 1995). Many distinct interaction mechanisms may be invoked to explain these occurrences, as suggested by numerical modelling and

* Corresponding author.
E-mail address: s.tonarini@igg.cnr.it (S. Tonarini).

0024-4937/$ – see front matter © 2008 Elsevier B.V. All rights reserved.
doi:10.1016/j.lithos.2008.09.012

the results of laboratory studies using synthetic analogues of silicate magmas (e.g., Folch and Martì, 1998; Weinberg and Leitch, 1998; Clynne, 1999; Couch et al., 2001; Perugini et al., 2002; Petrelli et al., 2006, and references therein). Two main mechanisms are generally distinguished on the basis of mineralogical and geochemical evidence, namely mingling and mixing. Mingling is a hybridisation process among magmas in which the composition of constituents remains identifiable. Mixing occurs when two or more chemically distinct magmas homogenise, giving rise to a new hybrid melt in which only chemical zoning in phenocrysts and/or mineralogical disequilibrium can yield information on the process which occurred (e.g., Bateman, 1995; Clynne, 1999, and references therein). However, textural features of mineralogical disequilibrium have recently been interpreted as due to convection within a single magma body heated from below and cooled from above, a process called self-mixing that has been reproduced experimentally for an andesitic lava from La Soufrière Hills volcano at Montserrat (Couch et al., 2001).

Whatever the mechanism responsible for magma mingling/mixing, these processes have been proved to play a fundamental role in triggering volcanic eruptions, because they generate an overpressure in the magmatic plumbing systems (e.g., Sparks et al., 1977; Huppert et al., 1982; Folch and Martì, 1998; Streck and Grunder, 1999; Murphy et al., 2000; Nagakawa et al., 2002; Suzuki and Nakada, 2007). Detailed petrographic, mineral chemistry, geochemical and isotopic investigations on volcanic rocks spanning the history of a volcano can be variably combined in order to define the role of mingling and/or mixing among other magmatic processes. Investigations aimed at identifying and defining the role of magmatic processes, in particular magma mingling/mixing, which have operated in the feeder systems are thus essential for long-term volcanic hazard assessment.

The Astroni volcano formed between 4.1 and 3.8 ka BP (Isaia et al., 2004, and references therein) within the Campi Flegrei caldera, in the northwestern portion of an area affected by volcano-tectonic collapse during the Agnano–Monte Spina eruption (4.1 ka; de Vita et al., 1999; Fig. 1). It is a well-preserved edifice constructed through a close sequence of at least 7 eruptions that generated pyroclastic deposits and lava domes of trachytic (s.l.) composition named Units 1 through 7. These rocks show macro- and microscopic evidence of mingling/mixing processes (e.g., Di Girolamo et al., 1984; Beccaluva et al., 1990; Isaia et al., 2004). A detailed geochemical and isotopic characterisation of these volcanic rocks ordered according to their stratigraphic succession could be used to track the evolution of magma both over time and during single eruptions, and to assess the role of processes such as crystallisation and magma mingling/mixing, and the possible involvement of shallow systems, i.e. continental crust, alteration products, hydrothermal systems (e.g., Orsi et al., 1995; Civetta et al., 1997; de Vita et al., 1999; Pappalardo et al., 1999, 2002; Pabst et al., 2007). Astroni volcanic activity thus provides a unique opportunity to shed light on low-pressure evolution processes and the nature of components feeding the Phlegraean magmatic system in recent times. Such information is very important also because the Astroni volcano is the best example of long-lasting activity from a single

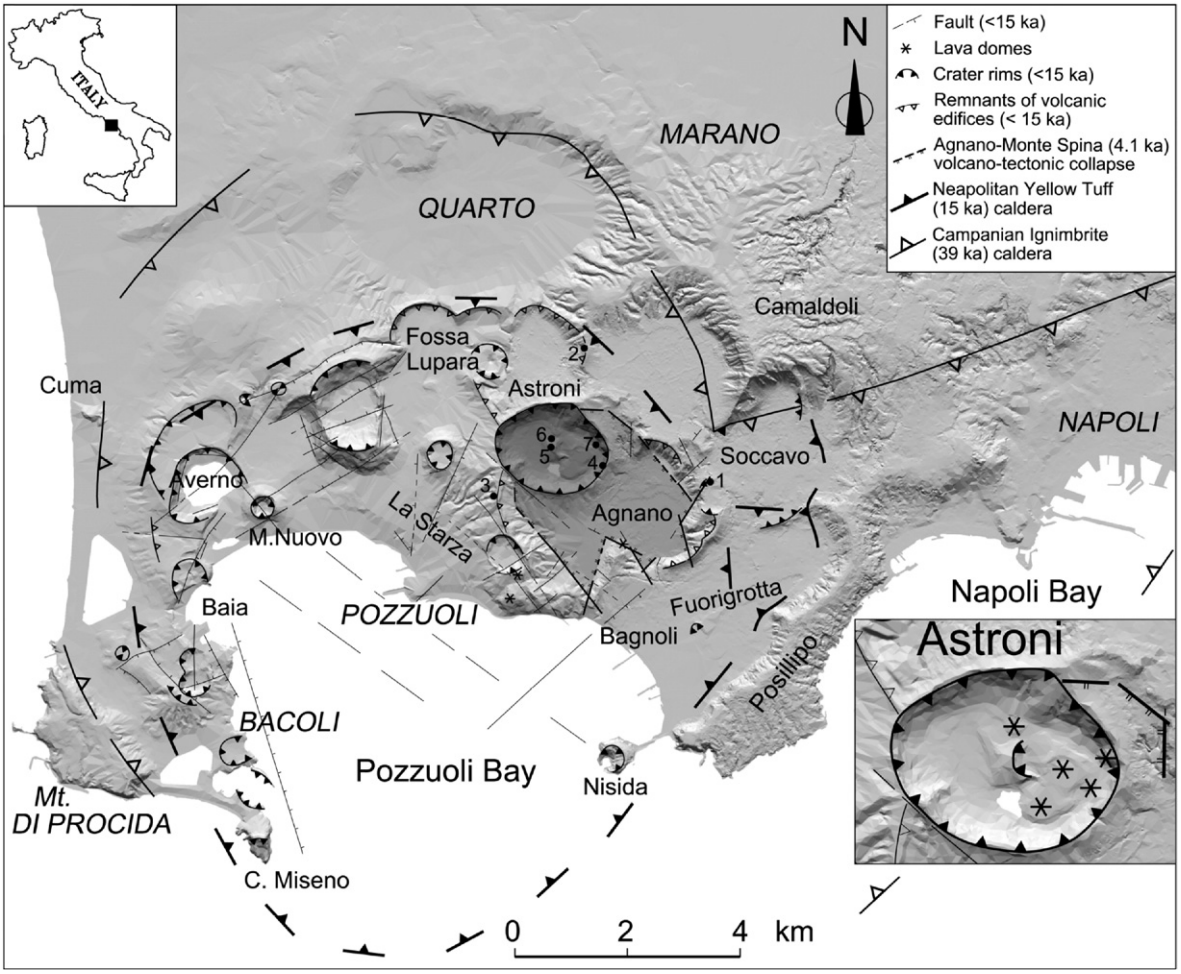

Fig. 1. Structural sketch map of the Campi Flegrei caldera showing the location of the Astroni volcano. The darker area includes the area collapsed during the Agnano–Monte Spina eruption. Sampling localities, marked with numbered dots, are: 1 — Monte Sant'Angelo; 2 — Contrada Romano; 3 — Celle; 4 — Cratere Astroni; 5 — Colle Imperatrice; 6 — Rotondella; 7 — Caprara.

vent area within the Campi Flegrei caldera (Isaia et al., 2004). Furthermore, the eruptive activity that built up the volcano, and in particular the event generating Unit 6, is considered one of the reference events for the medium-size expected event in the case of renewed volcanism at the Campi Flegrei caldera in the short- to mid-term (Orsi and Di Vito, unpublished data).

In this paper we present the results of bulk rock major and trace element analyses and of the isotopic investigation of a suite of samples representative of the Astroni volcano stratigraphic sequence. The volcanological implications of mingling/mixing processes at the Astroni volcano are evaluated, bearing in mind that long-term volcanic hazard assessment also depends on the ability to reliably constrain magma accumulation rates and pre-eruptive conditions.

1.1. Volcanological and petrological outline of the Astroni volcano within the Neapolitan volcanic area

Campi Flegrei is a Quaternary volcanic field in the Neapolitan volcanic area, which also includes the city of Naples (Fig. 1). It is located within a crustal sector currently affected by a regional extensional tectonic regime subsequent to the intense compressive phases that determined the collision between the Adria–Ionian

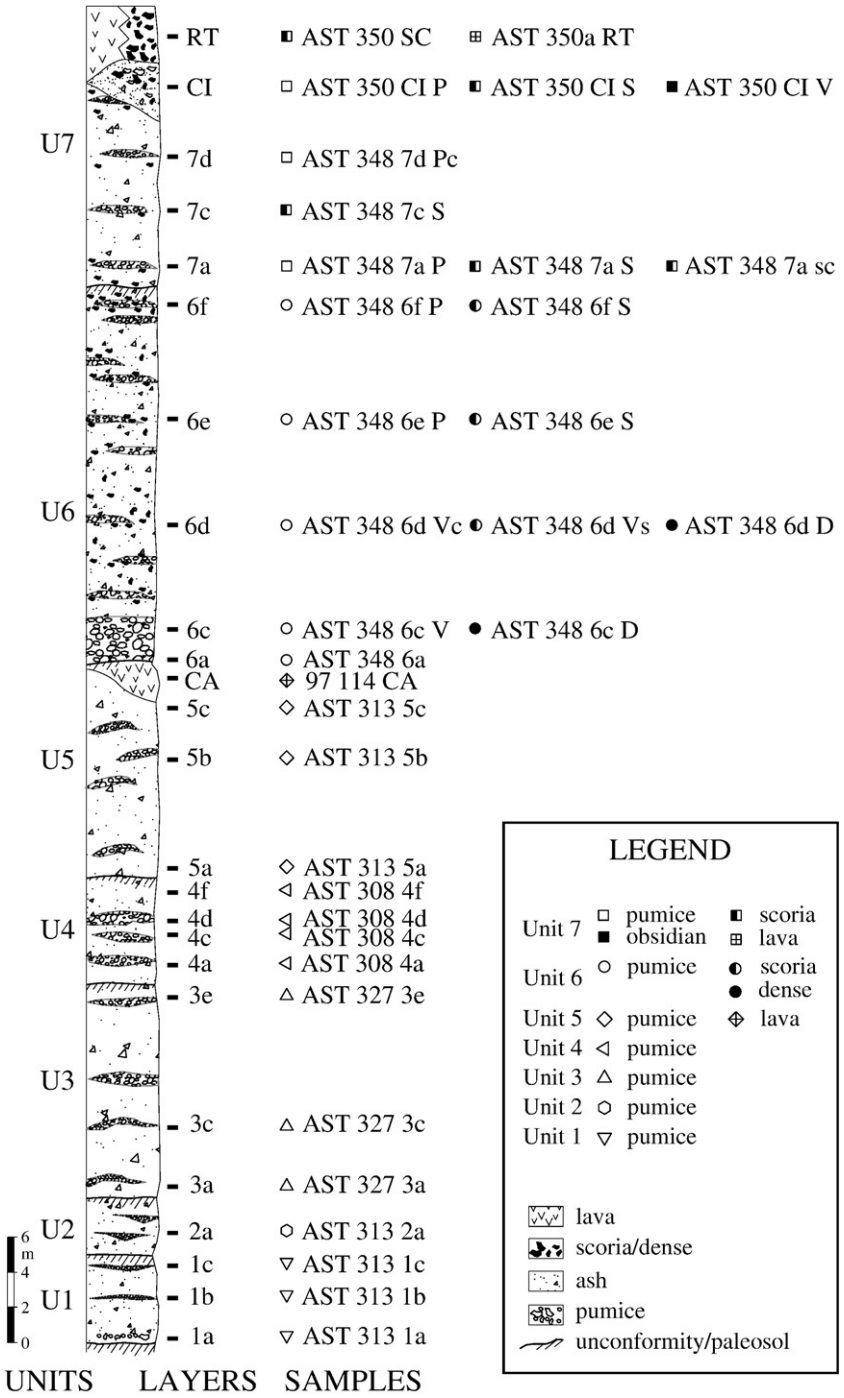

Fig. 2. Reconstructed type-sequence of the seven Astroni units (redrawn after Isaia et al., 2004). The samples collected from the different stratigraphic positions are labelled and identified with different symbols (the same ones used in all the geochemical and isotopic diagrams).

Table 1
Major oxide and trace element contents in selected Astroni volcanic rocks

Sample (AST)	313 1a	313 1b	313 1c	313 2a	327 3a	327 3c	327 3e	308 4a	308 4c	308 4f	313 5a	313 5c
Sampling locality	Contrada Romano	Contrada Romano	Contrada Romano	Contrada Romano	Celle	Celle	Celle	Mt. St. Angelo	Mt. St. Angelo	Mt. St. Angelo	Contrada Romano	Contrada Romano
Unit, layer $	1, a	1, b	1, c	2, a	3, a	3, c	3, e	4, a	4, c	4, f	5, a	5, c
Lithotype	Pumice fragments	Pumice fragments	Pumice fragments	Pumice fragments	Pumice fragments	Pumice fragments	Pumice fragments	Pumice fragments	Pumice fragments	Pumice fragments	Pumice fragments	Pumice fragments
Classification*	Phonolite/ trachyte	Phonolite	Phonolite	Phonolite	Trachyte	Phonolite	Phonolite	Phonolite	Phonolite	Phonolite	Phonolite	Phonolite
SiO_2	57.21	57.64	57.61	57.51	57.86	57.70	57.34	57.09	57.30	57.41	57.31	57.08
TiO_2	0.46	0.46	0.48	0.45	0.44	0.45	0.46	0.47	0.47	0.46	0.47	0.48
Al_2O_3	18.32	18.48	18.46	18.44	18.51	18.50	18.52	18.51	18.49	18.45	18.66	18.58
Fe_2O_3tot	4.41	4.29	4.48	4.28	4.16	4.20	4.46	4.47	4.39	4.26	4.48	4.54
MnO	0.12	0.12	0.13	0.12	0.12	0.12	0.12	0.12	0.12	0.12	0.12	0.12
MgO	0.86	0.85	0.87	0.82	0.77	0.81	0.94	0.93	0.90	0.89	0.97	1.02
CaO	3.26	3.10	3.06	3.10	3.02	3.04	3.42	3.39	3.26	3.20	3.49	3.62
Na_2O	4.06	4.01	4.23	4.06	4.09	4.09	3.94	3.94	3.93	3.97	3.91	3.88
K_2O	8.04	8.15	8.04	8.23	8.36	8.33	8.31	8.14	8.23	8.29	8.26	8.28
P_2O_5	0.16	0.17	0.16	0.17	0.15	0.17	0.18	0.17	0.15	0.16	0.18	0.20
LOI	3.00	2.64	2.35	2.71	2.42	2.50	2.25	2.69	2.68	2.70	2.09	2.15
Total	99.90	99.91	99.87	99.89	99.90	99.91	99.94	99.92	99.92	99.91	99.94	99.95
Be	13.0	12.2	13.4	12.5	12.3	12.6	11.2	11.6	12.1	12.3	10.4	11.0
V	67	67	66	67	63	65	72	73	72	75	77	79
Cr	5.21	b.d.l.	b.d.l.	5.89	5.85	5.51	b.d.l.	5.23	5.68	6.29	b.d.l.	b.d.l.
Co	5.36	5.32	4.99	5.04	4.74	4.80	5.67	5.62	5.51	5.60	6.00	6.02
Cu	9.15	8.93	9.33	8.98	8.75	8.48	8.52	9.54	9.41	11.24	9.44	9.55
Zn	87	83	89	84	82	84	83	90	91	91	87	79
Ga	20.6	20.5	20.3	19.5	18.5	19.8	19.9	20.1	20.5	19.6	20.3	19.1
Ge	1.49	1.38	1.48	1.42	1.41	1.37	1.40	1.35	1.34	1.40	1.37	1.30
As	26.0	25.1	27.0	26.7	25.2	26.2	23.2	25.6	25.1	24.5	22.7	21.5
Rb	362	360	357	357	346	357	331	341	343	345	337	325
Sr	415	466	346	439	435	447	533	512	513	512	591	587
Y	30.5	29.6	32.1	30.1	29.0	29.7	29.0	30.3	29.7	29.0	29.6	27.3
Zr	404	398	413	391	377	390	374	369	382	370	371	341
Nb	53	52	54	51	49	50	48	50	50	49	47	46
Mo	5.91	5.66	6.21	5.75	5.39	5.71	5.05	5.56	5.58	5.53	5.16	4.67
Sn	4.58	4.85	4.44	4.52	4.70	4.93	4.72	4.21	4.49	4.63	4.14	4.17
Sb	1.20	1.39	1.23	1.29	1.16	1.27	1.19	1.24	1.23	1.12	1.07	1.07
Cs	24.6	23.6	25.0	23.2	23.0	23.3	22.4	22.5	22.6	22.9	22.2	21.4
Ba	410	515	286	460	460	468	665	586	589	618	766	823
La	84	80	82	77	75	78	78	79	78	79	77	75
Ce	158	148	154	147	143	145	146	145	145	150	145	143
Pr	16.6	15.5	16.2	15.5	15.2	15.4	15.8	15.7	15.6	15.7	15.2	15.5
Nd	59	57	59	56	53	53	55	56	56	54	54	55
Sm	10.38	9.88	10.05	9.19	9.07	9.57	9.76	10.18	9.84	9.63	9.43	9.56
Eu	1.98	2.08	1.94	1.94	2.03	2.01	2.24	2.23	2.23	1.96	2.17	2.36
Gd	8.20	7.24	7.55	7.15	7.15	6.85	7.04	7.33	7.26	7.77	7.59	7.15
Tb	1.12	1.04	1.11	0.96	1.01	0.98	1.04	1.03	1.07	1.10	0.96	0.99
Dy	5.97	5.44	5.47	5.27	5.29	5.21	5.68	6.06	5.77	5.58	5.84	5.64
Ho	1.01	0.96	1.04	0.94	0.98	0.94	0.99	1.02	1.04	1.04	0.93	0.98
Er	3.03	2.87	3.23	2.63	2.72	2.75	2.73	2.74	2.89	2.99	2.78	2.65
Tm	0.43	0.42	0.45	0.44	0.42	0.43	0.43	0.39	0.39	0.47	0.42	0.38
Yb	3.15	2.97	3.36	3.08	2.92	2.84	3.01	2.90	2.95	3.14	2.96	2.88
Lu	0.47	0.48	0.47	0.40	0.45	0.41	0.42	0.42	0.43	0.45	0.39	0.37
Hf	8.62	8.29	8.85	8.45	8.31	8.35	8.52	8.59	8.43	8.38	8.11	7.77
Ta	3.41	3.25	3.67	3.19	3.25	3.20	3.27	3.24	3.26	3.21	3.02	3.04
W	7.30	7.17	8.14	7.52	7.98	7.63	7.33	7.05	6.93	7.68	6.82	6.97
Pb	59	58	62	59	58	58	57	56	55	58	52	53
Bi	0.40	0.36	0.35	0.40	0.34	0.33	0.34	0.39	0.31	0.30	0.31	0.33
Th	39.7	37.2	42.7	38.1	37.9	38.1	35.1	33.5	34.4	37.8	33.2	33.2
U	13.0	12.0	13.6	11.9	12.0	11.8	10.8	11.1	11.2	11.5	10.5	10.8
D.I.	80.00	80.52	80.71	80.85	81.50	81.30	79.41	79.15	79.77	80.35	78.85	78.42

The three-digits number in each sample label refers to a sampling locality indicated in the map of Fig. 1. $ for description of eruption characteristics, see Isaia et al. (2004).
*TAS classification (Le Maitre, 1989). Major oxide concentrations as wt.%; trace element concentrations as ppm.
D.I. = normative or + ab + ne. B.d.l. = below detection limit.

continental/oceanic plate and the European continental plate in the Miocene to Pleistocene (e.g., Elter et al., 2003; Sartori, 2003).

Volcanic activity at Campi Flegrei started more than 60 ka ago (Pappalardo et al., 1999) with a number of mainly explosive eruptions culminating in two high-magnitude, caldera-forming eruptions which generated the Campi Flegrei caldera. The oldest of such events is the Campanian Ignimbrite eruption (39 ka; more than 200 km^3 DRE; Fisher et al., 1993; Civetta et al., 1997; De Vivo et al., 2001; Fedele et al., 2003; Ort et al., 2003), whereas the youngest is the Neapolitan Yellow Tuff eruption (15 ka; more than 40 km^3 DRE; Orsi et al., 1992, 1995; Wohletz et al., 1995; Deino et al., 2004). The Neapolitan Yellow Tuff event was followed by three epochs of volcanic activity (15–9.5, 8.6–8.2, and 4.8–3.8 ka), with at least 72 smaller eruptions occurring from vents located either within the Neapolitan Yellow Tuff caldera floor or along its structural boundary (Di Vito et al., 1999; Orsi et al., 2004). After a quiescence of about 3000 years, the last eruption in 1538 AD produced the Monte Nuovo tuff cone (Di Vito et al., 1987). The Neapolitan Yellow Tuff caldera is affected by an

348 6a	348 6c V	348 6c D	348 6e P	348 6e S	348 6f P	348 6f S	348 7a P	348 7a sc	348 7d Pc	350 CI V	350 RT
Cratere Astroni	Cratere Astroni	Cratere Astroni	Cratere Astroni	Cratere Astroni	Cratere Astroni	Cratere Astroni	Cratere Astroni	Cratere Astroni	Cratere Astroni	Colle Imperatrice	Colle Imperatrice
6, a	6, c	6, c	6, e	6, e	6, f	6, f	7, a	7, a	7, c	Imperatrice	Rotondella
Pumice fragments	Pumice fragments	Dense fragments	Pumice fragments	Scoria fragments	Pumice fragments	Scoria fragments	Pumice fragments	Single scoria fragment	Pumice fragments	Obsidian fragments	Lava
Phonolite	Tephri-phonolite	Phonolite	Tephri-phonolite	Latite	Phonolite	Trachyte	Phonolite	Phonolite/ trachyte	Phonolite	Phonolite	Trachyte
56.98	55.43	57.93	55.93	56.69	56.47	57.18	57.13	56.88	57.07	57.87	58.47
0.46	0.55	0.48	0.54	0.54	0.50	0.51	0.49	0.48	0.46	0.49	0.49
18.68	18.41	19.00	18.64	18.84	18.72	18.87	18.89	18.59	18.80	18.97	19.48
4.37	5.27	4.43	5.37	5.17	4.78	4.92	4.50	4.46	4.35	4.61	4.53
0.12	0.12	0.12	0.12	0.11	0.12	0.12	0.12	0.11	0.11	0.12	0.11
0.91	1.59	0.98	1.55	1.38	1.10	1.16	0.96	1.03	0.91	1.01	0.91
3.36	4.84	3.64	4.77	4.38	3.91	4.00	3.60	3.76	3.42	3.60	3.29
3.87	3.55	3.98	3.63	4.65	3.89	4.66	3.87	4.13	3.90	3.95	3.68
8.34	7.78	8.27	7.98	6.45	7.96	6.52	8.41	7.71	8.52	8.55	8.09
0.18	0.28	0.20	0.29	0.24	0.23	0.23	0.21	0.20	0.18	0.19	0.18
2.67	2.20	0.93	1.19	1.56	2.30	1.79	1.80	2.63	2.24	0.62	0.73
99.94	100.02	99.96	100.01	100.01	99.98	99.96	99.98	99.98	99.96	99.98	99.96
11.1	9.7	11.4	8.8	8.9	10.0	10.1	10.2	10.3	10.4	10.6	9.2
72	108	77	109	99	87	93	82	76	81	85	77
b.d.l.	20.7	b.d.l.	15.63	8.18	6.12	5.13	b.d.l.	b.d.l.	7.30	7.37	b.d.l.
5.10	8.55	5.54	8.43	7.34	5.94	6.41	5.72	6.22	5.76	6.19	5.85
7.23	12.94	8.35	12.33	12.38	9.09	10.13	8.51	8.93	8.27	8.69	8.23
78	81	83	84	77	82	77	85	85	86	81	73
18.1	18.9	19.7	19.5	18.6	18.4	19.2	19.5	17.9	19.1	18.4	19.4
1.20	1.32	1.28	1.37	1.33	1.51	1.39	1.33	1.28	1.23	1.29	1.30
21.5	19.6	22.1	18.8	16.7	23.6	21.4	21.5	14.2	20.9	20.2	17.3
328	309	334	312	323	316	338	343	234	336	329	352
584	797	601	822	794	673	730	685	695	703	703	679
27.7	27.0	27.2	28.6	27.2	27.3	27.8	27.9	26.4	27.7	26.9	22.1
348	303	350	308	304	329	332	353	319	341	322	336
47	43	47	44	44	46	46	49	43	47	45	47
5.07	4.65	5.34	4.74	3.67	5.70	4.29	5.10	2.85	5.28	5.03	2.77
4.07	3.92	4.34	4.13	3.68	3.91	3.87	4.42	3.51	4.26	3.82	2.73
1.05	0.87	1.10	0.89	0.89	1.05	0.89	1.02	0.82	1.02	1.00	0.91
21.3	18.1	21.7	19.1	19.7	20.6	20.9	21.3	18.8	20.7	21.2	22.1
779	1179	878	1309	1277	1028	1065	1057	1016	1047	1004	914
74	70	76	75	74	77	76	78	72	75	71	63
145	133	147	147	142	144	144	149	135	139	135	120
15.5	14.5	15.9	16.0	15.7	15.9	15.5	15.6	14.5	14.6	15.6	13.7
51	53	55	57	54	57	55	54	52	52	57	49
9.11	9.36	9.54	9.44	9.25	9.48	9.65	9.22	8.91	8.92	9.69	8.19
2.29	2.21	2.18	2.46	2.44	2.28	2.33	2.20	2.10	2.18	2.14	2.05
6.93	6.55	7.26	6.95	7.02	6.81	7.03	6.63	6.66	6.98	6.42	5.46
0.91	0.92	1.02	1.03	1.00	1.06	1.04	0.98	0.93	0.95	1.00	0.84
5.24	5.22	5.71	5.20	5.25	5.45	5.09	5.13	4.68	4.90	4.95	4.16
0.90	0.89	0.93	0.98	1.01	1.03	0.97	0.95	0.96	0.91	0.94	0.73
2.70	2.50	2.74	2.80	2.67	2.74	2.72	2.76	2.65	2.45	2.60	2.18
0.37	0.33	0.40	0.37	0.41	0.43	0.40	0.40	0.38	0.37	0.39	0.32
2.86	2.45	2.77	2.72	2.43	2.79	2.71	2.50	2.63	2.60	2.80	2.23
0.41	0.34	0.40	0.40	0.44	0.44	0.40	0.43	0.43	0.39	0.39	0.33
7.72	6.21	7.56	6.57	6.86	7.27	7.17	7.66	7.11	7.04	7.64	7.60
3.07	2.57	3.00	2.70	2.73	2.92	2.86	2.98	2.85	2.85	3.04	2.97
7.08	5.91	6.95	6.37	5.47	7.16	6.71	6.81	5.31	6.64	7.13	4.95
51	47	53	49	46	53	47	50	51	53	55	49
0.30	0.28	0.24	0.36	0.32	0.71	0.30	0.22	b.d.l.	0.27	0.19	b.d.l.
32.8	27.8	32.9	28.5	29.0	32.7	30.7	31.7	32.0	32.7	34.7	34.2
10.9	9.4	10.8	9.3	9.5	12.9	11.5	10.3	10.2	10.2	11.0	8.3
79.33	71.96	78.49	72.54	73.75	76.58	75.59	78.47	77.75	79.47	78.75	77.92

ongoing resurgence, which occurs through a simple shearing mechanism (Orsi et al., 1991, 1996, 1999a). Campi Flegrei caldera is an active structure, as testified by the recent episodes of unrest in 1969–72 and 1982–84 (Corrado et al., 1977; Barberi et al., 1984, 1989; Orsi et al., 1999a,b), which produced a maximum uplift of about 3.5 m at Pozzuoli harbour, and by the widespread fumaroles and thermal spring activity (Allard et al., 1991; Caliro et al., 2007). The recent volcanic activity has generated mostly explosive eruptions of variable magnitude, some of which have followed each other in close succession within the same vent area (Orsi et al., 2004; Orsi and Di Vito, unpublished data). Astroni volcano is the best example of such long-lasting activity.

Astroni volcano formed towards the end of the 4.1–3.8 ka time interval (see discussion in Isaia et al., 2004). It was built up through 7 eruptions of variable magnitude characterised by phreatomagmatic and subordinate magmatic explosions. Only two events ended with low-energy explosions and lava extrusion. The deposits of the 7 eruptions are separated by erosional unconformities or thin paleosols containing evidence of Eneolithic settlements (Fig. 2) and suggesting

periods of inactivity between the eruptions. The units are composed of fine- to coarse-ash surge beds and subordinate fallout layers. The only Plinian coarse fallout layer occurs in Unit 6; it was dispersed eastward by an eruption column that reached a maximum height of about 20 km. The total volume of magma erupted during the seven Astroni events was 0.45 km^3 (DRE), whereas the total mass was $1.6*10^{12}$ kg (Orsi and Di Vito, unpublished data).

Previous petrological studies on the Campi Flegrei caldera have included only a few Astroni samples (e.g., Armienti et al., 1983; Di Girolamo et al., 1984; Rosi and Sbrana, 1987; Beccaluva et al., 1990; Civetta et al., 1991a; Di Filippo et al., 1991; D'Antonio et al., 1999). Geochemical and isotopic variability among Astroni products can be inferred from some of these studies (e.g., Di Girolamo et al., 1984; Rosi and Sbrana, 1987; Civetta et al., 1991a). Only Beccaluva et al. (1990) describe evidence of mineralogical disequilibria, which they discuss in the general framework of Campi Flegrei volcanism. None of these studies have investigated all seven Astroni units.

1.2. Sampling, sample preparation and analytical techniques

Thirty-four juvenile samples representative of the seven units in the stratigraphic sequence of the Astroni volcano were collected in different localities for mineralogical, petrographic, geochemical and isotopic investigation. Furthermore, one pumice sample (313 AMS SF 2a) from the Solfatara Tephra (Di Vito et al., 1999), underlying Astroni Unit 1 (Isaia et al., 2004), was also collected and analysed in order to better characterise the basal deposits of the Astroni sequence. The location of the sampled sequences is reported in Fig. 1, whereas the stratigraphic position of each collected sample within the reconstructed type-sequence is shown in Fig. 2. Both juvenile fragments from pyroclastic deposits and lava from lava domes were sampled. With the exception of one fallout layer at the base of Unit 6, the sampled pyroclastic beds are density-current deposits. One lava sample from the Caprara lava dome (97 114 CA; top of Unit 5), previously analysed by D'Antonio et al. (1999), is also reported in this work. Juvenile clasts with different degrees of vesiculation, from more vesiculated pumice to less vesiculated scoria and dense (i.e., poorly vesiculated glass) fragments, were found in Units 6 and 7. Fragments of each of these different types of juvenile clasts were collected and analysed separately as individual samples. Furthermore, one sample made up of obsidian fragments was also collected from Unit 7 and analysed separately. Each sample consisted of many juvenile clasts carefully selected on the basis of freshness. Sample AST 348 7a sc is a single, large scoria fragment from which glass and mineral phases were separated by handpicking under a binocular microscope in order to determine their Sr isotopic composition and highlight possible isotopic disequilibria. Representative juvenile clasts were selected for thin section preparation and petrographic observation. Prior to powdering, the clasts in each sample were cleaned with a dental drill equipped with a diamond disk in order to remove altered portions. Because sampling localities were close to the sea, the clasts were washed ultrasonically with de-ionised "Milli-Q" water to release possible traces of marine salt. The samples were then dried and ground in an agate mill.

Major oxide and trace element contents (Table 1) were determined by ICP-AES (major oxides) and ICP-MS (trace elements), respectively, at the Service d'Analyse des Roches et des Minéraux (S.A.R.M. — Centre de Récherche Pétrographiques et Géochimiques, Cedex, Nancy, France). Accuracy was checked against International Rock Standards; precision is 1–5% for most major oxides, and <10% for TiO_2 and P_2O_5. The precision of trace element determinations is generally <5% for contents higher than 100 ppm, <10% for contents between 50 and 100 ppm, and <20% for contents between 10 and 1 ppm (S.A.R.M. web site: http://crpg.cnrs-nancy.fr/SARM/index.html).

Sr and Nd isotopic compositions were determined using a Finnigan MAT 262 multicollector mass-spectrometer (at IGG-CNR, Pisa) after conventional ion-exchange procedures for Sr and Nd separation from the matrix. Measured $^{87}Sr/^{86}Sr$ ratios were normalised to $^{86}Sr/^{88}Sr=0.1194$, and $^{143}Nd/^{144}Nd$ ratios to $^{146}Nd/^{144}Nd=0.7219$. During the collection of isotopic data, replicate analyses of the NIST SRM 987 ($SrCO_3$) standard yielded an average $^{87}Sr/^{86}Sr$ ratio of 0.710200±0.000012 (2 SD, $N=15$), whereas replicate analyses of the La Jolla standard yielded an average $^{143}Nd/^{144}Nd$ ratio of 0.511851±0.000007 (2SD, $N=14$). All $^{87}Sr/^{86}Sr$ data were normalised to a value of 0.71025 for the NIST SRM 987 standard. Sr and Nd blanks were of the order of 0.3 ng during chemical analysis.

After alkaline fusion and boron separation and purification through ion-exchange procedures, B concentrations were determined by isotope dilution using the NIST SRM 952 spike. Reproducibility is estimated to be about 2.5% (Tonarini et al., 2003). The boron isotope composition was determined using a VG Isomass 54E positive thermal ionisation mass spectrometer after having separated boron through the ion-exchange procedures described in Tonarini et al. (1997). Accuracy was assessed through repeated analysis of the NIST SRM 951 standard throughout the full procedure and through replicate analysis of the GSJ-JB2 basalt reference standard (Tonarini et al., 2003). The isotopic composition of boron in samples is reported in the conventional delta notation ($\delta^{11}B$) as the per mil (‰) deviation from the accepted composition of NIST SRM 951 (certified $^{11}B/^{10}B=4.04362$; Catanzaro et al., 1970). The reproducibility of isotopically homogenous samples treated with alkaline fusion chemistry is approximately ± 0.5‰ (Tonarini et al., 2003), and this value is the analytical uncertainty assigned to the data presented in Table 2.

2. Results

2.1. Petrography

The juvenile products of all Astroni units (pumice, scoria, dense and obsidian fragments, and lavas) are porphyritic and glomeroporphyritic. The main paragenesis consists of abundant alkali-feldspar, plagioclase, pale green clinopyroxene, and subordinate biotite, iron oxide, rare leucite and apatite. The scoria fragments differ in that they are generally much less vesicular than pumice fragments and contain leucite in the groundmass, sometimes as microphenocrysts. Leucite has never been reported among the products of Astroni activity in previous petrological studies on the Campi Flegrei, whereas it has been reported in the less evolved products of the Agnano–Monte Spina eruption (Di Girolamo et al., 1984; Rosi and Sbrana, 1987). Banded pumice fragments occur frequently in the deposits of Units 6 and 7, where mm-sized bands containing more abundant vesicles and microlites in the groundmass alternate with others containing fewer vesicles and microlites. Alkali-feldspar and plagioclase are by far the predominant phenocrysts in the juvenile fragments of Units 1 through 4. Clinopyroxene abundance increases in the upper units, becoming equal to that of feldspars in some rocks. A pleochroic, dark green clinopyroxene, although subordinate, occurs along with the pale green variety in the uppermost layers of Units 3 and 4, and in Units 5 through 7. A colourless, third variety of clinopyroxene also occurs in Units 5 through 7, sometimes as microphenocrysts but more often as the core or rim of both normally and reversely zoned pale green individuals. Plagioclase, frequently with sieve-textured cores, is strongly zoned and in places rounded or corroded. Some alkali-feldspar phenocrysts are also corroded. All phenocrysts vary in size, without any clear correlation with the stratigraphic position of the samples. Alkali-feldspar generally ranges from 2.2 to 6.0 mm in size, but that in the Caprara and Rotondella lava domes reaches 1.5 and 0.5 cm in size, respectively. Plagioclase varies in size from 1.4 to 2.4 mm, and clinopyroxene from 0.9 to 3 mm. The groundmass of the pumice fragments is generally glassy and contains no resolvable microlites, whereas that of the scoria fragments varies from felty to intersertal and intergranular, with abundant microlites of feldspar,

Table 2
B, Sr and Nd isotope data on Astroni volcanic rocks

Sample	Unit	B (ppm)	$\delta^{11}B‰$	$^{87}Sr/^{86}Sr$	±2σ	$^{143}Nd/^{144}Nd$	±2σ
AST 350 RT wr	7			0.707341	0.000008	0.512488	0.000007
AST 350 CIV wr	7	42	−9.2	0.707395	0.000011	0.512484	0.000006
AST 348 7d Pc wr	7	35	−9.4	0.707315	0.000010	0.512492	0.000008
AST 348 7a sc. wr	7	35		0.707360	0.000009	0.512490	0.000008
AST 348 7a sc Sa	7			0.707540	0.000010		
AST 348 7a sc bt	7			0.707421	0.000011		
AST 348 7a sc dark green cpx	7			0.707417	0.000012	0.512443	0.000012
AST 348 7a sc pale green cpx	7			0.706638	0.000011	0.512544	0.000021
AST 348 7a sc glass	7			0.707380	0.000011		
AST 348 7a P wr	7	40		0.707310	0.000009	0.512489	0.000011
AST 348 6f S wr	6			0.707346	0.000012		
AST 348 6f P wr	6			0.707386	0.000010		
AST 348 6e S wr	6	34	−9.1	0.707291	0.000010	0.512506	0.000009
AST 348 6e P wr	6	41		0.707277	0.000009	0.512504	0.000007
AST 348 6c V wr	6	36	−9.8	0.707259	0.000011	0.512496	0.000010
AST 348 6c D wr	6	39	−9.7	0.707363	0.000011	0.512492	0.000007
AST 348 6a wr	6	48		0.707362	0.000010	0.512483	0.000009
AST 313 5c wr	5	45		0.707417	0.000008	0.512475	0.000009
AST 313 5a wr	5			0.707369	0.000009	0.512489	0.000008
AST 308 4f wr	4			0.707481	0.000008		
AST 308 4c wr	4			0.707470	0.000008		
AST 308 4a wr	4	39	−8.9	0.707471	0.000009	0.512474	0.000008
AST 327 3e wr	3			0.707510	0.000010		
AST 327 3c wr	3	49	−7.9	0.707510	0.000007		
AST 327 3a wr	3			0.707470	0.000008		
AST 313 2a wr	2	51	−8.3	0.707500	0.000009		
AST 313 1c wr	1			0.707537	0.000008		
AST 313 1b wr	1			0.707553	0.000007		
AST 313 1a wr	1	50	−8.1	0.707551	0.000010	0.512475	0.000008
Xenolith							
AST 348 L glass				0.706653	0.000011	0.512550	0.000011
AST 348 L cpx				0.706633	0.000012	0.512545	0.000011

wr = whole rock. Mineral abbreviations following Kretz (1983). Sample AST 348 L is a clinopyroxenitic xenolith collected from Unit 7.

leucite, clinopyroxene, iron oxide and glass. The groundmass of the dense fragments is felty to hyalopilitic or pilotaxitic, with variable amounts of feldspar microlites. Alteration is rare; the juvenile fragments only occasionally contain scattered calcite and/or hematite clots, clay minerals in alkali-feldspar phenocrysts (Unit 1), and rare chlorite and iron oxide partially replacing biotite. Leucite is variably analcimised. A more detailed petrographic description of the studied samples from each of the seven units is found in Isaia et al. (2004).

2.2. Major oxide and trace element geochemistry

Major oxide, trace element contents of representative rock samples of the different juvenile products in the seven Astroni units are reported in Table 1 and Appendix A. All the analysed rocks belong to a silica-undersaturated, mildly potassic alkaline series, because they contain normative nepheline (except sample AST 350 SC, which is corundum- and hypersthene-normative) and $Na_2O-2.0<<K_2O$ (Le Maitre, 1989). In the total alkali vs. silica classification diagram (TAS, Fig. 3) samples thus plot mostly in the phonolite and trachyte fields, with only one in the latite and two in the tephriphonolite fields. Interestingly, most of the pumice samples are classified as tephriphonolites and phonolites, whereas all the scoria samples are classified as latites and trachytes; the dense and obsidian fragments are all phonolites, whereas the two lavas are trachytes. On the whole, Astroni volcanics show a restricted compositional range and fall in the evolved portion of the compositional field defined by the products of volcanism younger than the Neapolitan Yellow Tuff eruption and caldera collapse at Campi Flegrei (less than 15 ka, see inset in Fig. 3; e.g., D'Antonio et al., 1999; de Vita et al., 1999).

The Th content was chosen as a differentiation index for the analysed Astroni samples, because i) it was accurately determined (analytical uncertainty <5%), ii) its concentrations range widely from 28 to 43 ppm (increasing by ~54%), and iii) it behaves as an incompatible element in the entire rock sequence. The sample from the Solfatara Tephra (313 AMS SF 2a; Appendix A) is a phonolite, which underlies the Astroni sequence; as its TiO_2, MgO, and Fe_2O_3tot contents are higher than those of the Astroni phonolites, this sample was not plotted. Harker diagrams highlight different major oxide trends (Fig. 4). TiO_2, MgO, Fe_2O_3tot, CaO and P_2O_5 contents (the latter not shown in Fig. 4) decrease with increasing Th contents, whereas SiO_2 and Na_2O contents increase.

Some oxides show a peculiar behaviour. For instance, the TiO_2 and Fe_2O_3tot contents of the most evolved samples (i.e. those with the highest Th contents) are a little higher than those along the main trend of decrease. This can be ascribed to the accumulation of Ti-magnetite, as observed in thin section, especially in sample AST 313 1c, which shows several mm-sized opaque phenocrysts. The anomalously high V content of these rocks (see later) supports the accumulation hypothesis. The Rotondella scoria and lava samples (AST 350a RT and AST 350 SC, Appendix A) have high Al_2O_3 contents: since they also have anomalously high Ba and Sr contents, these features are likely due to alkali-feldspar accumulation, as confirmed by the petrographic data.

Although generally increasing with the degree of chemical evolution of pumice and dense fragments, the Na_2O content is higher than expected in most scoria samples, whereas it is lower in samples of Rotondella lava and scoria (AST 350a RT and AST 350 SC; Appendix A). The K_2O and Al_2O_3 contents first increase and then decrease slightly in the pumice, dense fragments and lava samples, although K_2O contents are generally lower in the scoria samples. A possible explanation for this anomalous behaviour will be discussed in Section 3.1.

The behaviour of trace elements varies according to the degree of chemical evolution (Fig. 5). Transition metals such as V (and others not shown in Fig. 5) behave as compatible elements, as typically observed in alkaline series formed through undisturbed fractional crystallisation: with the exception of the most evolved sample (AST 313 1c), which displays Ti-magnetite accumulation, transition metal contents decrease regularly in the entire Astroni suite. Other compatible trace elements are Sr, Ba and Eu (the latter not shown in Fig. 5); their concentrations decrease quite steadily

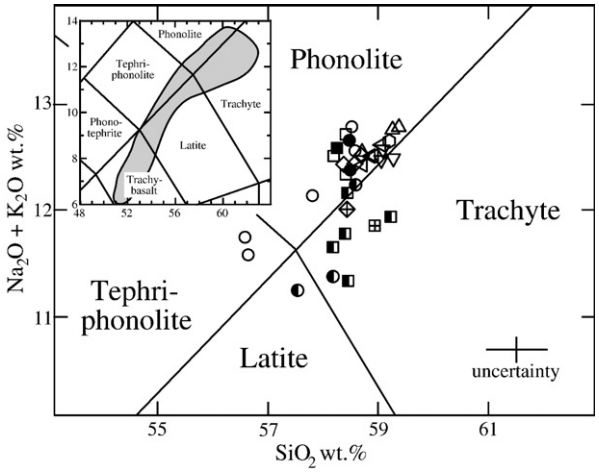

Fig. 3. Enlarged portion of the Total Alkali vs. Silica classification diagram (TAS, Le Maitre, 1989) for Astroni volcanics. Data from Table 1 and Appendix A. The grey area in the smaller plot encompasses the data field from the literature on Campi Flegrei volcanics younger than 39 ka (data from D'Antonio et al., 1999; de Vita et al., 1999; Pappalardo et al., 1999). Symbols as in Fig. 2.

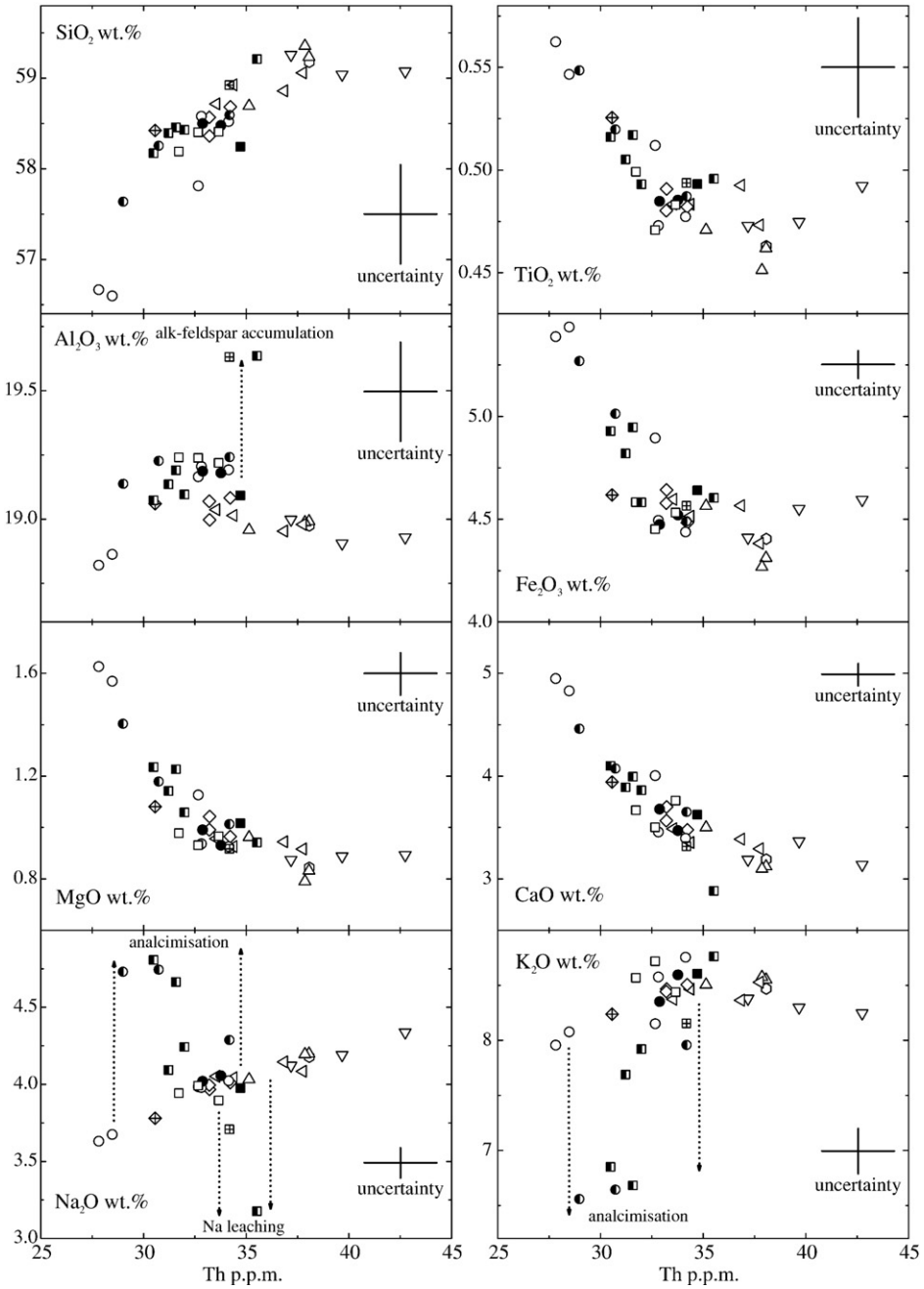

Fig. 4. Harker diagrams for Astroni volcanics. Major oxides (reported on a water-free basis) vs. Th. Data from Table 1 and Appendix A. The error bars are drawn considering the largest stated uncertainty for each element analysed at S.A.R.M. (see subsection 1.2). Symbols as in Fig. 2.

with increasing Th contents. Trace elements that behave as incompatible elements are Be, B, Rb, Y, Zr, Nb, Mo, Sn, Sb, REE (except Eu), Hf, Ta, W, Pb and Bi; their concentrations all increase more or less rapidly with increasing Th contents. Concentrations of Zr, Hf and Ta, the most incompatible trace elements, increase regularly throughout the entire Astroni suite. B contents vary within a narrow range from 34 to 52 ppm, and show a rough positive correlation with Th.

Most compatible and incompatible trace elements do not appear to discriminate among samples with different textures. However, Rb contents in scoria samples are unusual in that they are generally lower than those in pumice, dense fragments, and lava samples. Moreover, the Rotondella scoria sample (AST 350 SC) has unusually high Ba and, possibly, Sr contents, whereas the Rotondella lava sample (AST 350a RT) has a low La (as well as the other REE) content. These features will be discussed in subsection 3.1.

2.3. Sr, Nd and B isotope geochemistry

2.3.1. Whole rocks

Sr and Nd isotope data were determined on respectively 24 and 14 whole-rock samples representative of the entire Astroni stratigraphic sequence (Table 2). The variation in $^{87}Sr/^{86}Sr$ ratios (from 0.707277 ± 0.000010 to 0.707553 ± 0.000007) is significantly greater than the analytical uncertainty, whereas the variation in $^{143}Nd/^{144}Nd$ ratios (from 0.512506 ± 0.000009 to 0.512474 ± 0.000008) is only slightly greater than the error. The Sr and Nd isotope ratios of Astroni volcanics both overlap with part of the range of Campi Flegrei volcanics younger

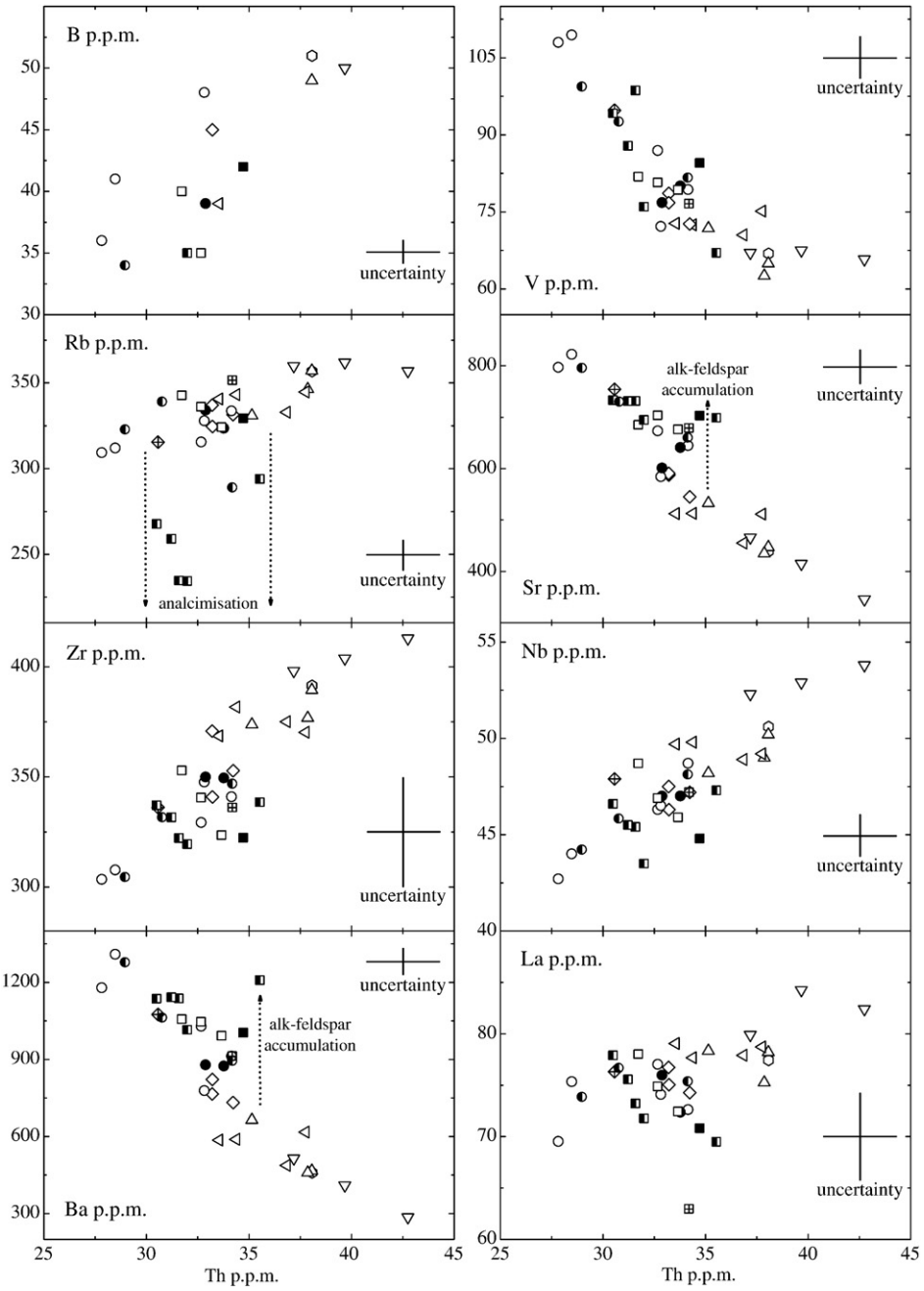

Fig. 5. Harker diagrams for Astroni volcanics. Trace elements vs. Th. Data from Table 1, Appendix A and Table 2 (for B contents). The error bars are drawn considering the largest stated uncertainty for each element analysed at S.A.R.M. (see subsection 1.2). Symbols as in Fig. 2.

than 39 ka ($^{87}Sr/^{86}Sr$: from 0.70729 to 0.70864; $^{143}Nd/^{144}Nd$: from 0.51254 to 0.51240; Tonarini et al., 2004; D'Antonio et al., 2007). The $\delta^{11}B$ values measured on 9 samples (Table 2) range from −7.9‰ to −9.8‰, once again overlapping with the range of Campi Flegrei volcanics younger than 39 ka (from −6.8‰ to −10.6‰). In particular, Unit 1 samples have the highest measured $^{87}Sr/^{86}Sr$ ratios, with an average value of 0.70755; Unit 3 samples have slightly variable $^{87}Sr/^{86}Sr$ ratios ranging from 0.707470 to 0.707510, and Unit 4 samples have a constant $^{87}Sr/^{86}Sr$ ratio of 0.70747; conversely, Unit 5 samples show variable $^{87}Sr/^{86}Sr$ ratios ranging from 0.707417 to 0.707369. The largest variation in $^{87}Sr/^{86}Sr$ ratios was found in Unit 6 samples, with values ranging from 0.707386 to 0.707259; the $^{87}Sr/^{86}Sr$ ratios of Unit 7 samples also vary significantly from 0.707395 to 0.707310. Interestingly, such variations in the three isotope ratios are well correlated with the degree of chemical evolution. In Fig. 6, the whole-rock $^{87}Sr/^{86}Sr$, $^{143}Nd/^{144}Nd$ and $\delta^{11}B$ values are plotted against the Th content, revealing good linear co-variation trends. In particular, $^{87}Sr/^{86}Sr$ and $\delta^{11}B$ values are positively correlated with Th, whereas $^{143}Nd/^{144}Nd$ is negatively correlated with Th.

2.3.2. Mineral separates

Sr and Nd isotopic analyses were carried out on mineral and glass separates from sample AST 348 7a sc (Unit 7, Table 2), a scoria sample characterised by evident mineralogical disequilibria. Pyroxene and glass from a pyroxenitic xenolith (Unit 6, Table 2) found in layer 6c were also separated and analysed. The obtained data clearly indicate Sr and Nd isotopic disequilibria between the minerals and glass: the $^{87}Sr/^{86}Sr$ ratio for sanidine is higher than the whole-rock value (0.70754 vs. 0.70736) and close to that measured in whole-rock samples from Units 1 and 2 (0.70750–0.70755). Biotite has a $^{87}Sr/^{86}Sr$ ratio of 0.707421 which is still

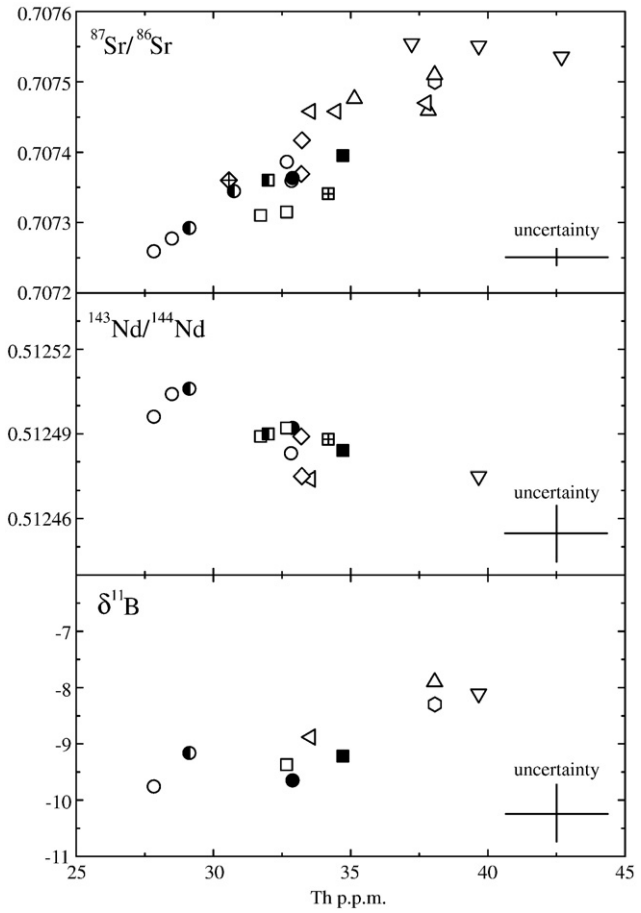

Fig. 6. $^{87}Sr/^{86}Sr$, $^{143}Nd/^{144}Nd$ and $\delta^{11}B$ vs. Th content diagrams for whole-rock Astroni volcanics. Data from Table 1, Appendix A and Table 2. Symbols as in Fig. 2.

higher than the whole-rock value. The glass has a $^{87}Sr/^{86}Sr$ ratio that is similar to that of the whole-rock (0.707380). More complex Sr and Nd isotope ratios are observed in the pyroxenes. The two varieties of clinopyroxene coexisting within the rock (one dark green, the other pale green) were separated in quantities sufficient for isotope analysis. The Sr and Nd isotope ratios of dark green clinopyroxene are slightly higher than those of the whole-rock. The Sr and Nd isotope ratios measured in he pale green clinopyroxene ($^{87}Sr/^{86}Sr$=0.706638; $^{143}Nd/^{144}Nd$=0.512544) are very different from those of the entire Astroni whole-rock sequence, but identical to those measured in the pale green clinopyroxene and glass of the pyroxenitic xenolith ($^{87}Sr/^{86}Sr$=0.70665–0.70663; $^{143}Nd/^{144}Nd$=0.512550–0.512545).

2.3.3. Chemostratigraphy

The chemostratigraphy of Astroni products (Fig. 7) indicates that the early products of Unit 1 are the most evolved of the entire Astroni sequence, varying slightly from trachytes to phonolites (average Th content of ~42 ppm). The composition of products in Units 2 through 5 remains phonolitic; however, they become progressively less evolved, with Th contents decreasing from 38 to 33 ppm. The Caprara lava dome (Th ~31 ppm) at the top of Unit 5 is trachytic. The composition of products from Units 6 and 7 is more variable. Layers 6a through 6f change in composition from phonolitic to tephriphonolitic, with Th contents ranging from 33 to 28 ppm. The least evolved compositions in the Astroni sequence are found in layers 6c and 6e, which also display significant differences among the coexisting juvenile fragments of variable vesicularity. The Unit 7 products also show a slight chemical variability, ranging from trachytes to phonolites, with a general slight increase in the Th content up-section (31–35 ppm); however, these Th variations are within the analytical uncertainty. Note that the pumice juveniles are phonolites, whereas the coexisting scoria juveniles are trachytes. Unit 7, and thus Astroni activity, ends with the trachytes of the Rotondella scoria cone and lava dome.

The $^{87}Sr/^{86}Sr$ ratio and $\delta^{11}B$ vary roughly following the geochemical variations of Astroni products (Fig. 7). The variations in the Sr isotope ratio are significantly greater than the analytical uncertainty. In the products of Units 1 through 5, from the base upward, $^{87}Sr/^{86}Sr$ decreases from 0.70755 to 0.70734 and $\delta^{11}B$ decreases from −8 to −9‰. Interestingly, the $^{87}Sr/^{86}Sr$ ratio sharply decreases at the transition between the last layer of Unit 4 and the first layer of Unit 5. The products of Units 6 and 7 are also isotopically heterogeneous. The lowest $^{87}Sr/^{86}Sr$ and $\delta^{11}B$ values were measured in the pumice fragments of layers 6c and 6e (0.70726–0.70728 and −10‰, respectively), which are also the least evolved tephriphonolites. The Sr and B isotope ratios also vary in the other layers of Units 6 and 7, with values lower than those characterising Units 1 through 5; $^{87}Sr/^{86}Sr$ ranges from 0.70728 to 0.70740 and $\delta^{11}B$ from −9 to −10‰. It is noteworthy that coexisting juvenile fragments of pumice and scoria have distinct $^{87}Sr/^{86}Sr$ ratios, particularly in layers 6c, 6f, and 7a. As noted earlier, mineral separates from one sample of Unit 7 show significant Sr isotopic disequilibrium, with biotite and dark green clinopyroxene characterised by a $^{87}Sr/^{86}Sr$ ratio of ~0.70742, i.e. higher than that of glass (0.70738), whereas the Sr isotope ratio of sanidine is the same as that of the early products of Unit 1 (0.70754; Table 2).

3. Discussion

The complex variability of the petrographic, geochemical and isotopic data, as well as the chemostratigraphy of the analysed products, suggests that several magmatic, volcanic and post-eruption processes operated prior to, during and after the growth of the Astroni volcano. It is therefore important to identify these processes and assess the role of each one. The quite regular trends seen in the whole-rock major oxide and trace element Harker diagrams (Figs. 4 and 5) suggest that the magmas which fed Astroni activity may have evolved mainly via fractional crystallisation. Petrographic observations indicate that dominant alkali-feldspar, plagioclase and clinopyroxene (in decreasing order of abundance), and subordinate biotite, opaque minerals and apatite constitute the main fractionating phases. However, many lines of evidence suggest that open-system processes were operative in the Astroni magma plumbing system: the significant compositional variability of the products of Units 6 and 7 (tephriphonolites, latites, phonolites and trachytes) with respect to those of Units 1 through 5 (tephriphonolites and phonolites, with only two trachytes); the mineralogical disequilibria; the significant variation in Sr, Nd and B isotope compositions; the regular co-variation trends between isotope ratios and degree of chemical evolution (Tables 1 and 2; Figs. 3–7). Open-system magmatic processes such as crustal assimilation concomitant with fractional crystallisation (AFC), and interaction among differently evolved magma batches, i.e. mingling and/or mixing, can be envisaged. Regardless of the type of process, the nature of the end-members in the magmatic system needs to be characterised. Furthermore, the identification of possible relationships between these processes and the style of eruption throughout the growth of the Astroni volcano has remarkable implications on volcanic hazard assessment. All these topics will be addressed in the following subsections.

3.1. Low temperature alteration

The overall variations in the major and trace element contents of Astroni products, from less evolved tephriphonolites (and latites) to more evolved phonolites and trachytes (Figs. 3–5 and Table 1), might well be the result of dominant fractional crystallisation processes only. However, the peculiar variability of certain major oxides and trace elements (Figs. 4 and 5), outlined in Section 2.2, needs to be addressed.

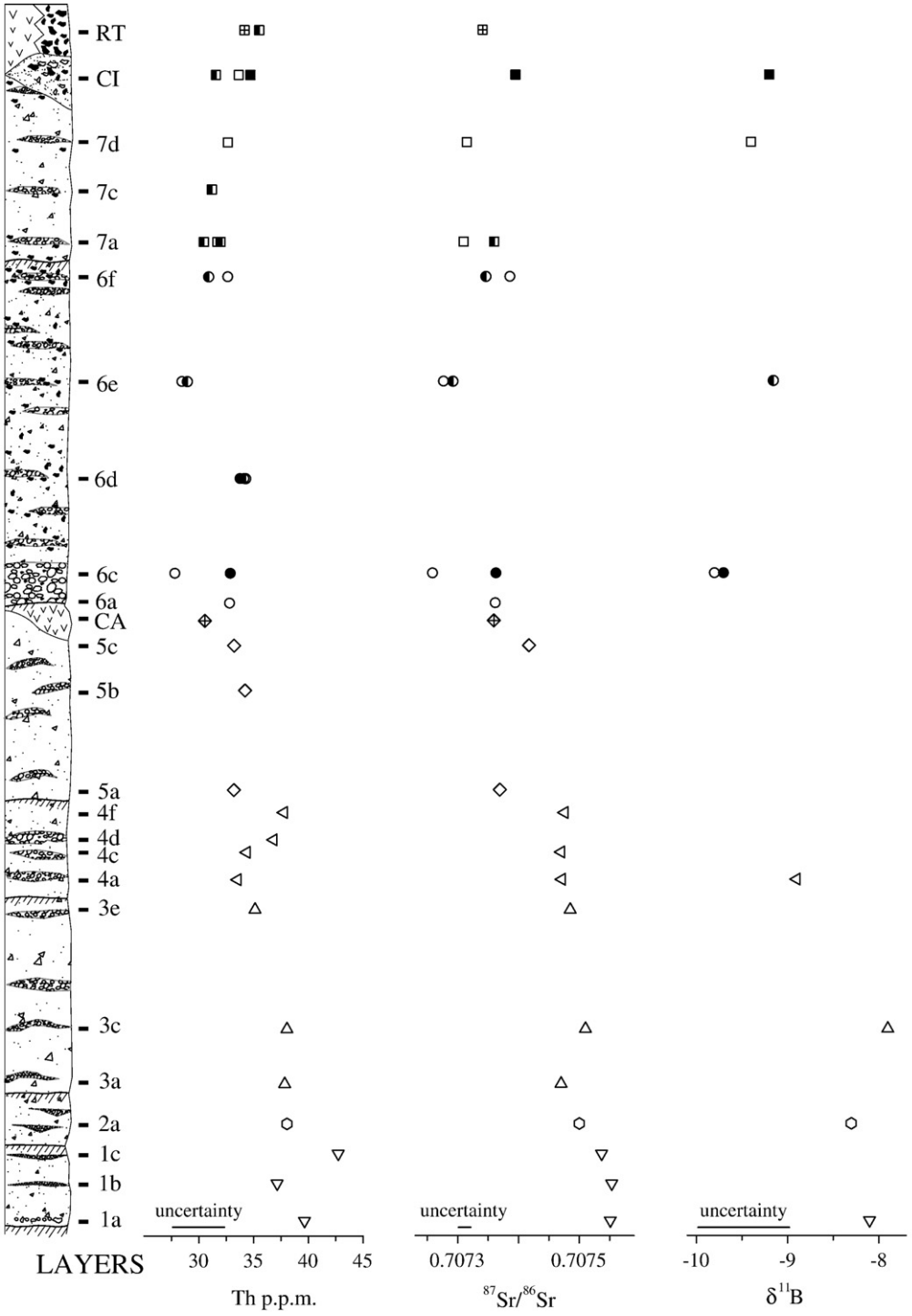

Fig. 7. Chemostratigraphy of Astroni volcanics. Data from Table 1, Appendix A and Table 2; $^{87}Sr/^{86}Sr$ value of sample 97 114 CA (Caprara lava dome) from Di Renzo et al., unpublished data. Symbols as in Fig. 2.

The low REE content in the Rotondella lava sample is not easily explained, since these elements are not fluid-mobile. Conversely, the anomalously high Na_2O and low K_2O and Rb contents of most scoria samples (Table 1 and Figs. 4 and 5) can be easily explained by analcimisation of leucite, a dissolution–reprecipitation mechanism which occurs at temperatures of 40 to 150 °C (Putnis et al., 2007, and references therein). This process has been proven to determine significant uptake of Na and, occasionally, of Cs, accompanied by K and Rb loss by the host rocks, without mobilising other alkaline earth metals such as Sr and Ba (Prelević et al., 2004). The Astroni scoria sample with the lowest Rb content (234 ppm) also has the highest L.O.I. content (2.63 wt.%; AST 348 7a sc, Table 1). In some scoria samples (AST 348 6e S and AST 348 6f S) Rb does not show depletion, whereas K_2O does: this confirms that the geochemical variations induced by the analcimisation process are hard to predict due to the zeolitic behaviour of analcime (Prelević et al., 2004). Interestingly, the leucite in the Rotondella scoria (AST 350 SC) is fresh, and K_2O and Rb show no evidence of mobilisation. Conversely, this sample displays a significant loss of Na_2O and, to a lesser extent, of Cs; this loss was likely related to a syn- or post-emplacement process possibly occurring during

or after cooling of the Rotondella scoria cone, for example leaching by circulating fluids, as strongly suggested by the reddish hue of the products.

It is noteworthy that Rotondella samples (AST 348 6e S) affected by alkali loss or gain have indistinguishable B isotope compositions. This suggests that the analcimisation process has negligible effects on B systematics.

3.2. Fractional crystallisation

In the light of the previous discussion, analcimisation of leucite can be assumed to be the main process responsible for lowering the total alkali content of Astroni scoria samples with respect to those of the corresponding phonolitic pumice samples, so that they plot in the latite and trachyte fields (Fig. 3). The possible fractional crystallisation trends identified for the Astroni products (Fig. 8) must have started from less evolved tephriphonolites, giving way to more evolved phonolites or trachytes. In order to quantitatively test the fractional crystallisation processes, mass balance calculations (XLFRAC; Stormer and Nicholls, 1978) and Rayleigh fractionation modelling were performed using whole-rock major oxide and trace element contents, respectively (Table 1, Appendix A), and available mineral compositional data on Astroni products (D'Antonio et al., unpublished data). Electronic copies of representative fractionation models can be found online in Appendix B; the models are also schematically depicted as parent–daughter transitions in the TAS diagram (Fig. 8).

For the fractional crystallisation processes, tephriphonolite AST 348 6c V (Unit 6) was chosen as the parent magma, because it is the least evolved of the analysed Astroni rocks (Th=27.8 ppm; Table 1). Several evolved rocks can be chosen as daughter magmas in the model. The most evolved Astroni sample is the AST 313 1c (Unit 1) phonolite (Th=42.7 ppm; Table 1). The modelled transition between the chosen parent magma and this phonolite (Fig. 8a) yielded very good results (Appendix B): the process requires ~29 wt.% crystallisation of a mineral assemblage made up of dominant sanidine (13.3 wt.%) and plagioclase (6.8 wt.%), and lower amounts of clinopyroxene (4.3 wt.%), biotite (2.5 wt.%), Ti-magnetite (1.6 wt.%) and apatite (0.7 wt.%). These calculated amounts match the relative percentage of each type of phenocryst observed in the rocks reasonably well. This, and the low value of the sum of the squares of residuals ($\sum r^2$=0.06), suggests the plausibility of such a fractional crystallisation process. Use of the Rayleigh fractionation equation to model the transition between the same two rocks yielded good matches between observed and calculated trace element contents (differences were within the analytical uncertainty of each trace element; Appendix B), thereby supporting the results of major oxide modelling.

The transitions from the same parent magma (=sample AST 348 6c V) to other evolved Astroni rocks, i.e. phonolite AST 327 3a (Th=37.9 ppm; Table 1) in Unit 3 (Fig. 8b), phonolite AST 348 6d Vc in Unit 6 (Fig. 8c) and trachyte AST 313 1b in Unit 1 (Fig. 8d), were also modelled; the good results confirm the importance of fractional crystallisation in the evolution of Astroni magmas (see Appendix B). Conversely, all attempts to model the fractional crystallisation process using the composition of scoria samples as either parent or daughter magmas gave unsatisfactory results, because of the high $\sum r^2$ and accumulation of all six main mineral phases (up to 32 wt.%). These results confirm the profound chemical changes caused by analcimisation of leucite.

3.3. Crustal contamination and magma mingling/mixing

The results of major oxide and trace element modelling indicate that a liquid line of descent from a tephriphonolitic to phonolitic magma, represented by the pumice samples of Units 1 through 5, is likely. However, fractional crystallisation alone can explain neither the significant isotopic variations among Astroni samples, nor the mineralogical and isotopic disequilibria (differences in the $^{87}Sr/^{86}Sr$ of whole-rocks, glass and phenocrysts) detected in the products of Units 6 and 7. In order to constrain the nature of open-system processes, trace element and isotope variations (with particular attention to B geochemistry) are discussed in the following.

Magmas feeding Campi Flegrei caldera volcanism younger than the Campanian Ignimbrite were affected by crustal contamination processes at mid-crustal depths (10–20 km) and by magma mingling/mixing processes at shallower depths, as indicated by geochemical and isotopic data (D'Antonio et al., 1999; de Vita et al., 1999; Pappalardo et al., 2002; Tonarini et al., 2004; D'Antonio et al., 2007). It may thus be useful to compare the isotopic features of the analysed Astroni samples with those of samples representative of earlier Campi Flegrei volcanic activity. In particular, in the following diagrams (Figs. 9–12) isotopic data (Tonarini et al., 2004; D'Antonio et al., 2007) on representative samples

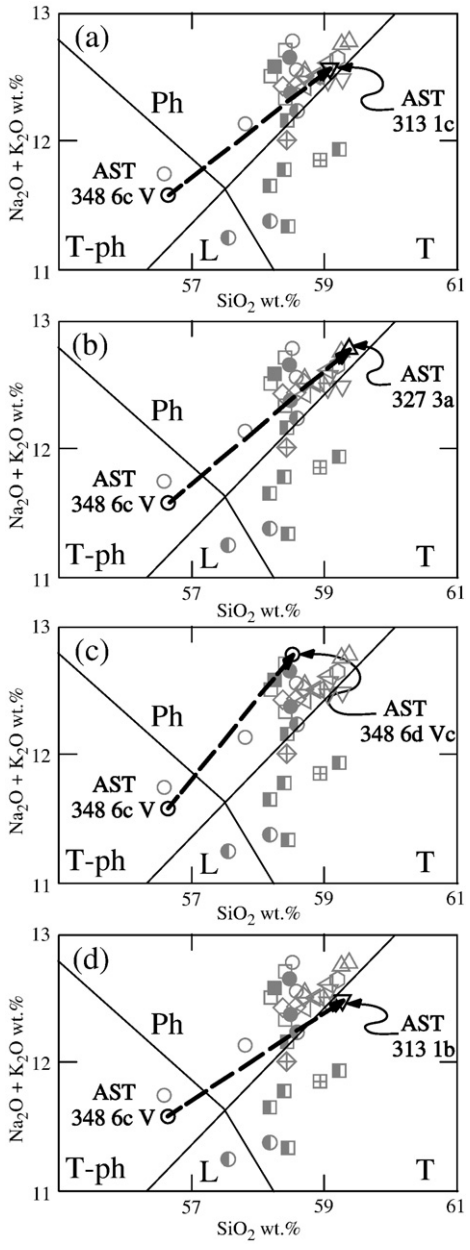

Fig. 8. Portion of the TAS classification diagram showing fractional crystallisation paths from parent to daughter magmas representative of less and more evolved Astroni samples used in XLFRAC modelling (numerical results reported in Appendix B). T-ph=tephriphonolite; Ph=phonolite; L = latite; T = trachyte. Symbols as in Fig. 2. See Section 3.2 for discussion.

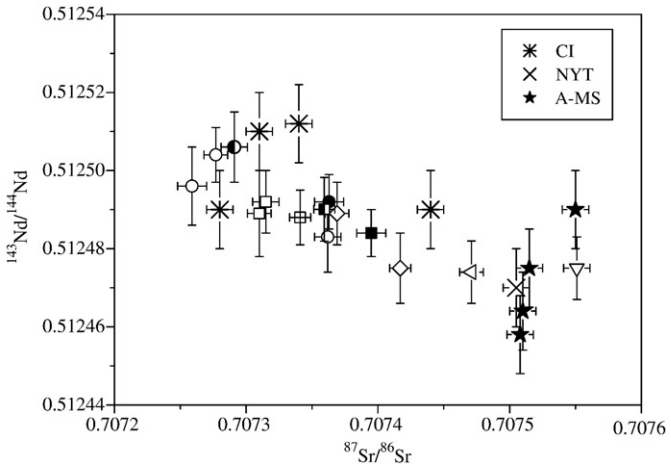

Fig. 9. $^{87}Sr/^{86}Sr$ ratio vs. $^{143}Nd/^{144}Nd$ ratio diagram. Data from Table 2. Symbols for Astroni samples as in Fig. 2. Data for Campanian Ignimbrite (CI), Neapolitan Yellow Tuff (NYT) and Agnano–Monte Spina (A–MS) products from D'Antonio et al. (2007).

of eruptions at Campi Flegrei in the 39.1–3.8 ka time span were plotted for comparative purposes; among these, samples representative of the Campanian Ignimbrite, Neapolitan Yellow Tuff and Agnano–Monte Spina eruptions are identified with different symbols.

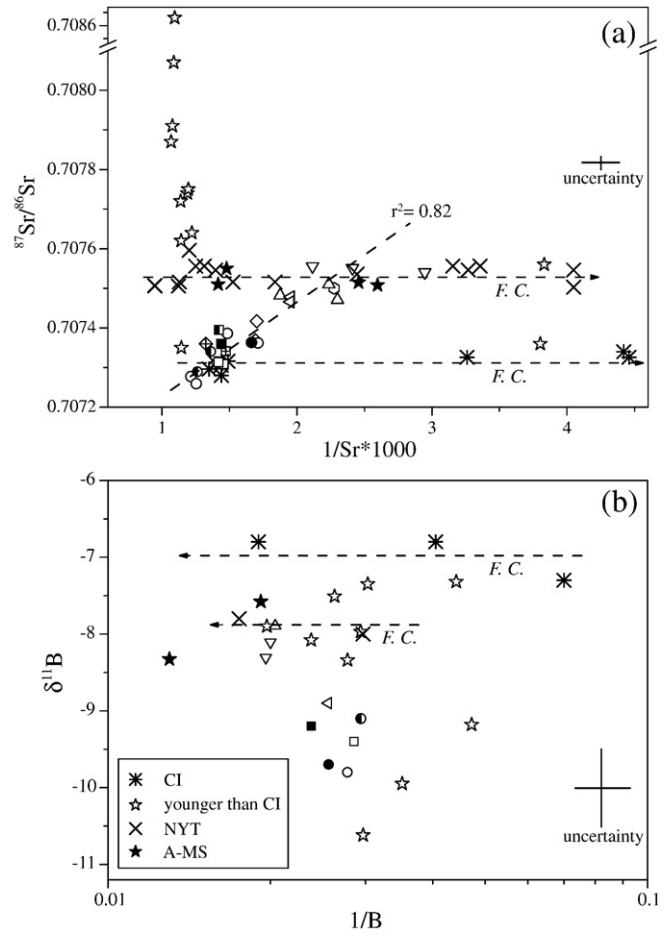

Fig. 10. (a): $^{87}Sr/^{86}Sr$ vs. 1/Sr*1000 diagram. (b): $\delta^{11}B$ vs. 1/B diagram. Data for Astroni volcanics from Tables 1 and 2. Symbols as in Fig. 2. F.C. = fractional crystallisation. The error bars for trace elements are drawn considering the largest stated uncertainty for each element analysed at S.A.R.M. (see subsection 1.2). Data for Campanian Ignimbrite, Neapolitan Yellow Tuff, Agnano–Monte Spina, and products younger than Campanian Ignimbrite (39 ka) from Civetta et al. (1997), Orsi et al. (1995) and D'Antonio et al. (2007).

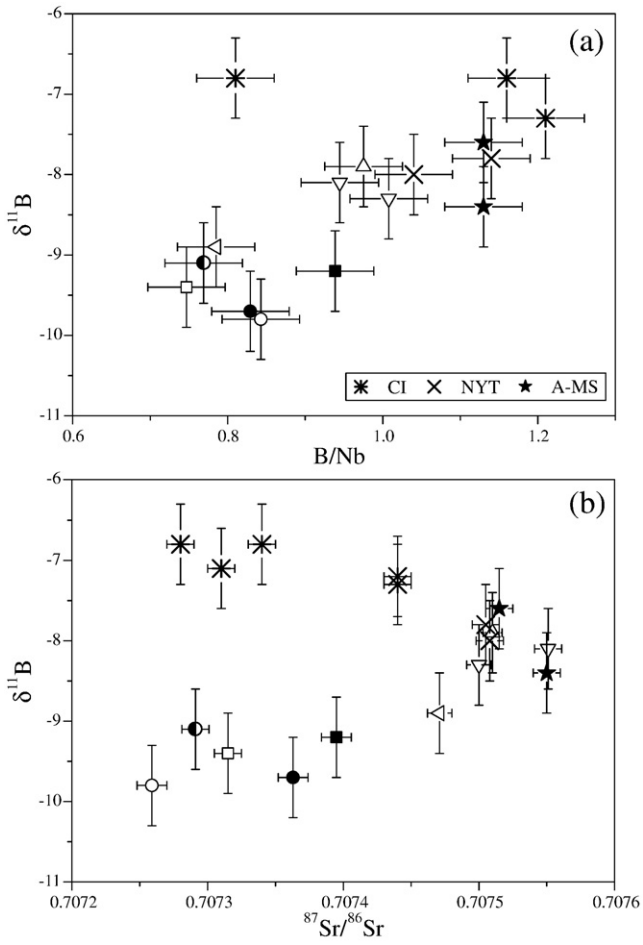

Fig. 11. (a): $\delta^{11}B$ vs. B/Nb ratio diagram. (b): $\delta^{11}B$ vs. $^{87}Sr/^{86}Sr$ ratio diagram. Data for Astroni volcanics from Tables 1 and 2. Symbols for Astroni samples as in Fig. 2. Data for Campanian Ignimbrite, Neapolitan Yellow Tuff and Agnano–Monte Spina products from D'Antonio et al. (2007).

The products of Astroni activity are characterised by roughly anti-correlated $^{87}Sr/^{86}Sr$ and $^{143}Nd/^{144}Nd$ ratios (Fig. 9). This anti-correlation suggests the involvement of two isotopically distinct end-members, one with lower Sr and higher Nd isotope ratios, the other with higher Sr and lower Nd isotope ratios. Interestingly, Astroni Sr and Nd isotope ratios

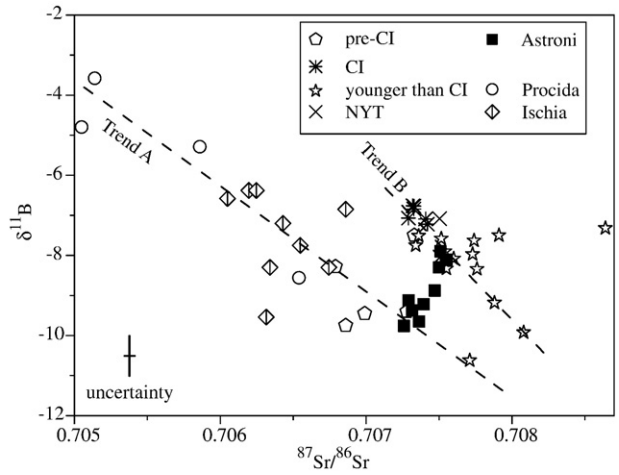

Fig. 12. $^{87}Sr/^{86}Sr$ versus $\delta^{11}B$ diagram. Data for Astroni volcanics from Table 2. Data for Phlegraean Volcanic District volcanics from Tonarini et al. (2004) and D'Antonio et al. (2007). See subsection 3.4 for discussion on Trend A and Trend B.

vary between those of the Campanian Ignimbrite and Neapolitan Yellow Tuff (Orsi et al., 1995; Civetta et al., 1997; Pappalardo et al., 2002; Tonarini et al., 2004; D'Antonio et al., 2007). Furthermore, the Sr and Nd isotope ratios measured in the products of Units 1 through 4 ($^{87}Sr/^{86}Sr$ = 0.707553–0.707470 and $^{143}Nd/^{144}Nd$ = 0.512474) are indistinguishable from those of the products of the Agnano–Monte Spina eruption ($^{87}Sr/^{86}Sr$ = 0.707556–0.707470; $^{143}Nd/^{144}Nd$ = 0.51246–0.51249; de Vita et al., 1999; D'Antonio et al., 2007). The less evolved and more evolved end-members involved in Astroni activity thus appear to be isotopically similar to the Campanian Ignimbrite and to both Neapolitan Yellow Tuff and Agnano–Monte Spina products, respectively.

$^{87}Sr/^{86}Sr$ vs. 1/Sr*1000 (Fig. 10a) and $\delta^{11}B$ versus 1/B (Fig. 10b) plots can help understand the relative role played by closed- and open-system evolution processes affecting the magmas which fed the Astroni volcano. In the $^{87}Sr/^{86}Sr$ vs. 1/Sr*1000 plot, the samples of Astroni Units 1 through 4, Neapolitan Yellow Tuff and Agnano–Monte Spina describe a unique fractional crystallisation trend at a $^{87}Sr/^{86}Sr$ ratio of about 0.7075, whereas samples of the Campanian Ignimbrite and of one post-Campanian Ignimbrite sample define another fractional crystallisation trend at a $^{87}Sr/^{86}Sr$ value of about 0.7073. The remaining samples display a near-vertical trend between the Campanian Ignimbrite trachyte (with the lowest $^{87}Sr/^{86}Sr$ values) and the Minopoli 2 trachybasalt (with the highest Sr isotope ratio and content). The Astroni rocks of Units 5 through 7 fall close to the Campanian Ignimbrite trachytic samples, whereas all Astroni rocks define a positive trend connecting the Campanian Ignimbrite and the Neapolitan Yellow Tuff fractional crystallisation trends. The positive trend described by Astroni rocks (r^2 = 0.82; Fig. 10a) could be accounted for by interaction of an evolved magma, similar to the least evolved Campanian Ignimbrite melt, with a more evolved Neapolitan Yellow Tuff- or Agnano–Monte Spina-like magma through mingling/mixing processes. The observed trend may alternatively be explained by selective crustal contamination and/or assimilation of country rock during magma ascent. As already proposed by Pappalardo et al. (2002) and D'Antonio et al. (2007), assimilation of the Calabrian Hercynian crust (average $^{87}Sr/^{86}Sr$ = 0.7146 and Sr = 298 ppm; Caggianelli et al., 1991) could explain the moderate increase in $^{87}Sr/^{86}Sr$ accompanying magma differentiation.

The applicability of the AFC hypothesis to the evolution of magmas which fed Astroni has been checked through the analysis of B isotopic compositions and contents (Fig. 10b). Astroni products display a negative correlation trend between a less evolved, low B (<30 ppm) and $\delta^{11}B$ (< −10‰) end-member and a more evolved, high B (>50 ppm) and $\delta^{11}B$ (>−8‰) end-member. The less evolved end-member has a $\delta^{11}B$ value close to that of Pigna San Nicola and Minopoli 1 magmas, but with a significantly lower $^{87}Sr/^{86}Sr$ ratio (0.7073), whereas the more evolved end-member has a $\delta^{11}B$ close to that of the evolved Neapolitan Yellow Tuff- and Agnano–Monte Spina-like magmas and a $^{87}Sr/^{86}Sr$ ratio of about 0.7075. The open-system evolution of Astroni magmas was thus driven toward a high $^{87}Sr/^{86}Sr$ end-member characterised by a high B content. Since the average B content is about 5 ppm in the lower continental crust (Leeman et al., 1992) and about 15 ± 10 ppm in the upper continental crust (Taylor and McLennan, 1985), the high $^{87}Sr/^{86}Sr$, high-B end-member of the Astroni trend cannot be identified as the continental crust. On the other hand, B is strongly partitioned into silicate melts relative to all common equilibrium mineral phases, and its partition coefficient is close to those of highly incompatible elements (Brenan et al., 1998). This means that B is strongly enriched in the more evolved melts: its content in the Campi Flegrei samples can be in excess of 100 ppm (Tonarini et al., 2004). Moreover, the high B content, coupled with the high $\delta^{11}B$ and $^{87}Sr/^{86}Sr$ values, is inconsistent with shallow contamination by seawater, since the latter has high $\delta^{11}B$ and $^{87}Sr/^{86}Sr$ values (~+40‰ and 0.7091) but low B and Sr contents (~5 and 8 ppm). Contamination by limestone can also be ruled out because i) no limestone lithics have been found in the Astroni products, and ii) modern marine carbonates have B contents ranging from 10 to 30 ppm, and $\delta^{11}B$ between +10 and +30‰ (Leeman and Sisson, 1996). Both B contents and isotopic compositions are strongly reduced during diagenesis, as demonstrated for Miocene calcarenites from the Maiella Mountains (Apulian platform, southern Italy) characterised by 2 ppm of B and a $\delta^{11}B$ of about +6‰ (Tonarini et al., 2003). In summary, significant crustal contamination to explain the B content, and $\delta^{11}B$ and $^{87}Sr/^{86}Sr$ variations in Astroni magmas can be clearly ruled out.

3.4. Magmatic end-members in the mingling/mixing process

Based on the above discussion, the geochemical and isotopic features of Astroni volcanics are clearly better explained through some interaction process involving two variably evolved and isotopically distinct magmatic end-members. In order to identify these end-members, several geochemical and isotopic parameters can be combined. It is noteworthy that $\delta^{11}B$ is positively correlated with not only the B content (Fig. 10b) but also the B/Nb ratio, a parameter which is not expected to vary during fractional crystallisation due to the similar degree of incompatibility of the two elements (Fig. 11a). The Campanian Ignimbrite trachyte, Neapolitan Yellow Tuff and Agnano–Monte Spina samples define the high $\delta^{11}B$ and B/Nb extreme of the trend defined by Astroni volcanics. Moreover, $\delta^{11}B$ is also positively correlated with the $^{87}Sr/^{86}Sr$ ratio, and the $\delta^{11}B$ and $^{87}Sr/^{86}Sr$ values are the lowest measured in the Astroni samples of Units 6 and 7 (Fig. 11b). The Astroni samples of Units 1 through 4 overlap with the Neapolitan Yellow Tuff and Agnano–Monte Spina products, whereas the Campanian Ignimbrite rocks show lower $^{87}Sr/^{86}Sr$ coupled with higher $\delta^{11}B$ values.

The more evolved magmatic end-member (with $^{87}Sr/^{86}Sr \geq 0.7075$, $\delta^{11}B \geq -8$‰ and $^{143}Nd/^{144}Nd \leq 0.51247$) was isotopically very similar to the magma that fed the Agnano–Monte Spina eruption a few hundred years earlier, and to the one that fed the Neapolitan Yellow Tuff eruption around 15 ka BP (Orsi et al., 1995; Tonarini et al., 2004; D'Antonio et al., 2007; Di Renzo et al., unpublished data). It was also characterised by high B and low Sr concentrations, likely acquired during fractional crystallisation in a shallow reservoir. The less evolved end-member shows similar $^{87}Sr/^{86}Sr$ (≤0.70726) and $^{143}Nd/^{144}Nd$ (≥0.51251) ratios but significantly different $\delta^{11}B$ values with respect to the Campanian Ignimbrite products (i.e., −9 to −10‰ for samples from Astroni Units 6 and 7, versus −7‰ for Campanian Ignimbrite rocks). The latter difference argues against the involvement of a Campanian Ignimbrite-like magma as an end-member in the mingling/mixing processes which produced Astroni magmas. To help identify the low-$\delta^{11}B$ Astroni end-member, it is useful to compare $\delta^{11}B$ and $^{87}Sr/^{86}Sr$ values of Astroni products with those of Phlegraean Volcanic District volcanics (Fig. 12; Tonarini et al., 2004; D'Antonio et al., 2007). In the B vs. Sr isotope diagram for Phlegraean Volcanic District volcanics, $\delta^{11}B$ decreases as $^{87}Sr/^{86}Sr$ increases according to two sub-parallel trends named Trend A and Trend B (D'Antonio et al., 2007). The low-$\delta^{11}B$ Astroni end-member falls along Trend A, defined by the Procida K-basalts, Ischia volcanics, Campi Flegrei volcanics older than Campanian Ignimbrite, and Pigna San Nicola and Minopoli 1 trachybasalts. Trend A has been interpreted as a mantle trend, possibly reflecting the progressive involvement of subducted sediment-derived melts in the mantle beneath the Phlegraean Volcanic District (Tonarini et al., 2004). The low-$\delta^{11}B$ Astroni end-member may represent a poorly evolved magma that ascended from this modified mantle source and resided at mid-crustal depths, where it differentiated into a trachyte. Trend B is defined by Campanian Ignimbrite and post-Campanian Ignimbrite products. As previously discussed by D'Antonio et al. (2007), the geochemical and isotopic features of the younger-than-39-ka Campi Flegrei rocks can be explained by 1–2% crustal contamination. Furthermore, shallow-level mingling/mixing processes between at least two distinct magmas, i.e. the Campanian Ignimbrite trachyte and a shoshonite similar to those feeding the Pigna San Nicola and Minopoli 1 eruptions, produce the observed trend. The high $\delta^{11}B$

Astroni end-member belongs to Trend B, as do the Neapolitan Yellow Tuff and Agnano–Monte Spina volcanics.

The Sr isotope compositions measured in mineral separates from Astroni Unit 7 (sample AST 348 7a sc in Table 2) indicate significant isotopic disequilibrium. Isotopic disequilibrium recorded by crystals from volcanic rocks is conventionally considered petrological evidence for magma mingling/mixing, especially when coupled with mineralogical disequilibrium (e.g., Cioni et al., 1995; de Vita et al., 1999; Perini et al., 2003; Ramos et al., 2005; Aulinas et al., 2007; Di Renzo et al., 2007). In sample AST 348 7a sc, the Sr isotopic disequilibria detected between sanidine ($^{87}Sr/^{86}Sr$=0.707540), biotite ($^{87}Sr/^{86}Sr$=0.707421), dark green clinopyroxene ($^{87}Sr/^{86}Sr$=0.707417) and glass ($^{87}Sr/^{86}Sr$=0.707380) suggest a mingling process involving crystals mostly equilibrated in the Neapolitan Yellow Tuff–Agnano–Monte Spina-like magma. Moreover, the similarity between the $^{87}Sr/^{86}Sr$ ratio of pale green clinopyroxene ($^{87}Sr/^{86}Sr$=0.706638) and that of glass ($^{87}Sr/^{86}Sr$=0.706653) and clinopyroxene ($^{87}Sr/^{86}Sr$=0.706633) separated from the clinopyroxenitic xenolith (AST 348 L in Table 2) suggests that loose crystals of a distinct, more mafic magma less enriched in radiogenic Sr were entrained and carried upward by Astroni magmas during ascent.

In summary, the geochemical and Sr, Nd, B isotope variability suggests that the erupted Astroni magmas mainly resulted from complex mixing and mingling processes involving: i) a mantle-derived magma evolved through fractional crystallisation in the mid-crustal reservoir(s), ii) a more evolved magma similar to those which fed the Neapolitan Yellow Tuff and Agnano–Monte Spina eruptions and residing at a shallower crustal level, and iii) loose crystals of a more mafic magma that were entrapped in the rising late Astroni magmas.

3.5. Magmatic processes and volcano growth

On the basis of the previous discussion on geochemical and isotopic data (Figs. 9–12), the variations in Th contents and Sr isotope ratios are likely the result of mingling processes between at least two magmatic end-members, one more evolved (phonolite), with higher radiogenic Sr and $\delta^{11}B$, and the other less evolved (tephriphonolite), with lower radiogenic Sr and $\delta^{11}B$. The detected chemical and isotopic variations with stratigraphic height (Fig. 7) corroborate this hypothesis and can be used to trace the magmatic and volcanic events that occurred during the growth of the Astroni volcano.

The concomitant decrease in both Th contents (from 43 to 31 ppm) and $^{87}Sr/^{86}Sr$ ratios (from 0.70755 to 0.70734) from Units 1 through 5 suggests that the first five Astroni eruptions were fed by magmas with varying geochemical and isotopic compositions. In particular, the overall variation in the Th content is only slightly greater than the analytical uncertainty, and no significant geochemical gap can be identified among the products of these lower units. In contrast, the variation in the Sr isotope ratio is more significant than that of the Th content, and significantly greater than the analytical uncertainty; moreover, this variation is not closely correlated with the stratigraphic height. Indeed, the Sr isotope ratio decreases from 0.70755, in the samples of Unit 1, to 0.70748, in those of Units 3 and 4. It then changes abruptly to 0.70737 between the uppermost layer in Unit 4 and the lowermost layer in Unit 5. The significant gap in the $^{87}Sr/^{86}Sr$ ratio is also accompanied by a slight decrease in the Th content from 37 to 33 ppm; however, this decrease is within the analytical uncertainty. Conversely, no other significant geochemical or isotopic gaps can be identified at the transitions between Units 5 and 6, and Units 6 and 7. The products of Units 6 and 7 exhibit scattered Th contents and Sr isotope ratios.

Since the products of Units 1 are geochemically and isotopically very similar to those of the uppermost units of the Agnano–Monte Spina eruption (de Vita et al., 1999; S. Tonarini, unpublished data), it can be hypothesised that the more evolved end-member was a batch of magma left in the feeder system after the Agnano–Monte Spina eruption. This hypothesis implies that the Agnano–Monte Spina magma was not completely extruded during the eruption and the coeval volcano–tectonic collapse.

Detailed analysis of the chemostratigraphy, in particular the Sr isotope stratigraphy, of Astroni products indicates that the magma mingling process was complex (Fig. 7). Prior to eruption 5, the Astroni feeder system, including the residue of the Agnano–Monte Spina magma, was invaded either by the less evolved magmatic end-member only, or also by another batch of magma with intermediate Sr isotopic composition (~0.70748). According to the available estimates on the timing of mingling events (e.g., Ramos et al., 2005; Browne et al., 2006), in both cases magma invasion likely occurred shortly before the start of Astroni volcanism, inducing mingling and triggering the onset of activity. In the case of only one magma input, the mingling event produced a magma with a Sr isotope ratio of about 0.70748 that fed the system during the emplacement of Units 1 through 4 (Fig. 7). The abrupt change in the Sr isotope ratio and in the Th content at the transition between Units 4 and 5 likely marks another mingling event between the mingled magma which fed the previous activity and the low radiogenic-Sr and $\delta^{11}B$ end-member. This new hybrid magma fed Astroni activity during the emplacement of Units 5 through 7. All the products of Units 6 and 7 vary slightly in geochemical and isotopic characteristics within the range of the mingled magma which fed Unit 5 and the low radiogenic-Sr and $\delta^{11}B$ end-member, without any clear temporal trend (Fig. 7). Moreover, they are characterised by the contemporaneous occurrence of juvenile fragments with different texture, vesicularity, and geochemical and isotopic features, as well as banded pumice fragments. The textural variability is likely the result of the variable eruption dynamics. Conversely, the geochemical and isotopic variability suggests extrusion of a hybrid melt, resulting from the intimate mingling, or almost complete mixing, of the two identified end-members until the end of Astroni activity. This hybrid magma carried many phenocrysts equilibrated in the less evolved end-member less enriched in radiogenic Sr and $\delta^{11}B$, as indicated by the strong Sr isotopic disequilibrium detected between phenocrysts and glass.

4. Summary and conclusions

The geochemical and isotopic investigation of Astroni products has allowed the reconstruction of the open-system evolution and identification of fractional crystallisation processes. In particular, mineralogical disequilibria, whole-rock B–Nd–Sr isotopic variations with the degree of chemical evolution and in time, as well as the significant Sr isotopic disequilibria between phenocrysts and glass, can be accounted for by mingling/mixing rather than crustal contamination. The geochemical and isotopic evidence suggests that mingling/mixing involved at least two main distinct magmatic end-members, one more evolved (phonolite), with higher radiogenic Sr and $\delta^{11}B$ contents, the other less evolved (tephriphonolite) and with lower radiogenic Sr and $\delta^{11}B$ contents. The chemostratigraphy also suggests the possible presence of an intermediate magmatic end-member characterised by a Sr isotope ratio intermediate between those of the two end-members. The intermediate end-member mingled with the more evolved end-member could have fed eruptions 1 through 4. The latter shows strong geochemical and isotopic similarities with the magmas that fed the final phases of the Agnano–Monte Spina eruption, which occurred a few hundred years earlier in the Astroni vent area. Since the Agnano–Monte Spina-like products erupted first, the early phases of Astroni activity were probably fed by the magma left in the system by the previous eruption. The less evolved end-member is likely a mantle-derived magma which evolved into a tephriphonolite through dominant fractional crystallisation. It, or alternatively the intermediate end-member, invaded the plumbing system and mingled with the resident Agnano–Monte Spina-like magma. In both hypotheses, mingling/mixing was the likely

triggering mechanism, at least for the onset of Astroni activity and for the beginning of eruption 5.

Astroni volcano can be taken as the best example of a sequence of eruptions very close in time, and from the same vent area, occurred at the Campi Flegrei caldera (Isaia et al., 2004; Orsi et al., 2004). Therefore, improvement of the current knowledge on the evolution of the volcano, including its magmatic feeder system, is an important step forward in the long-term volcanic hazards assessment of the Campi Flegrei caldera.

The presented data demonstrate that mingling/mixing events triggered at least two of the seven eruptions which build up the Astroni volcano. More detailed geochemical and isotopic data are required for a more exact reconstruction of links between the evolution of the magmatic feeder system, eruption dynamics and magma reservoir withdrawal. A better clarification of the role of mixing/mingling processes as triggering mechanism, and an estimation of the timing of mixing/mingling events for each of the seven Astroni eruptions would be achieved through more detailed geochemical and isotopic analyses, especially analytical profiles on zoned phenocrysts (e.g., Ramos et al., 2005; Browne et al., 2006; Suzuki and Nakada, 2007). Such data would also be extremely important in the identification of possible precursors to an eruption and, consequently, in short-term volcanic hazard assessment.

Acknowledgements

F. Dell'Erba and R. Isaia are kindly thanked for their helpful assistance during sampling. M.C. Andria is acknowledged for her help during sample preparation, and M. Serracino for skilful assistance during EMP analyses at IGAG in Rome. Many thanks to L. Civetta for her encouragement that spurred us to write this paper. Thanks also to William P. Leeman, an anonymous referee and the Editor-in-chief Andrew Kerr, for their critical review and constructive criticism. This work was financially supported by INGV-GNV grants 2002–2005 to S.T., M.D. and G.O.

Appendix A. Supplementary data

Supplementary data associated with this article can be found, in the online version, at doi:10.1016/j.lithos.2008.09.012.

References

Allard, P., Maiorani, A., Tedesco, D., Cortecci, G., Turi, B., 1991. Isotopic study of the origin of sulfur and carbon in Solfatara fumaroles, Campi Flegrei caldera. Journal of Volcanology and Geothermal Research 48 (1/2), 139–159.

Armienti, P., Barberi, F., Bizouard, H., Clocchiatti, R., Innocenti, F., Métrich, N., Rosi, M., Sbrana, A., 1983. The Phlegraean Fields: magma evolution within a shallow chamber. Journal of Volcanology and Geothermal Research 17, 289–311.

Aulinas, M., Civetta, L., Di Vito, M.A., Orsi, G., Gimeno, D., Férnandez-Turiel, J.M., 2007. The "Pomici di Mercato" Plinian eruption: magma chamber and eruption dynamics. Bulletin of Volcanology 70, 825–840.

Barberi, F., Corrado, G., Innocenti, F., Luongo, G., 1984. Phlegrean fields 1982–1984: brief chronicle of a volcano emergency in a densely populated area. Bulletin Volcanologique 47 (2), 175–185.

Barberi, F., Carapezza, M., Innocenti, F., Luongo, G., Santacroce, R., 1989. The problem of volcanic unrest: the Phlegraean fields case history. Atti dei Convegni Lincei 80, 387–405 (Rome).

Bateman, R., 1995. The interplay between crystallization, replenishment and hybridization in large felsic magma chambers. Earth Science Reviews 39, 91–106.

Beccaluva, L., Di Girolamo, P., Morra, V., Siena, F., 1990. Phlegraean fields volcanism revisited: a critical re-examination of deep eruptive system and magma evolutionary processes. Neues Jahrbuch für Geologie und Paläontologie Monatshefte 5, 257–271.

Brenan, J.M., Neroda, E., Lundstrom, C.C., Shaw, H.F., Ryerson, F.J., Phinney, D.L., 1998. Behaviour of boron, beryllium and lithium during melting and crystallization: constraints from mineral-melt partitioning experiments. Geochimica et Cosmochimica Acta 62, 2129–2141.

Browne, B.L., Eichelberger, J.C., Patino, L.C., Vogel, T.A., Uto, K., Hoshizumi, H., 2006. Magma mingling as indicated by texture and Sr/Ba ratios of plagioclase phenocrysts from Unzen volcano, SW Japan. Journal of Volcanology and Geothermal Research 154, 103–116.

Caggianelli, A., Del Moro, A., Paglionico, G., Pinarelli, L., Rottura, A., 1991. Lower crustal granite genesis connected with chemical fractionation in the continental crust of Calabria (Southern Italy). European Journal of Mineralogy 3, 159–180.

Caliro, S., Chiodini, G., Moretti, R., Avino, R., Granieri, D., Russo, M., Fiebig, J., 2007. The origin of the fumaroles of La Solfatara (Campi Flegrei, South Italy). Geochimica et Cosmochimica Acta 71, 3040–3055.

Catanzaro, E.J., Champion, C.E., Garner, E.L., Malinenko, G., Sappenfeld, K.M., Shields, W.R., 1970. Boric acid, isotopic, and assay standard reference materials. United States National Bureau of Standards Special Publication, vol. 260, pp. 17–70.

Cigolini, C., 1998. Intracrustal origin of Arenal basaltic andesite in the light of solid-melt interaction and related compositional buffering. Journal of Volcanology and Geothermal Research 86, 277–310.

Cioni, R., Civetta, L., Marianelli, P., Métrich, N., Santacroce, R., Sbrana, A., 1995. Compositional layering and syn-eruptive mixing of a periodically refilled shallow magma chamber: the AD 79 Plinian eruption of Vesuvius. Journal of Petrology 36 (3), 739–776.

Civetta, L., Carluccio, E., Innocenti, F., Sbrana, A., Taddeucci, G., 1991a. Magma chamber evolution under the Phlegraean Fields during the last 10 ka: trace element and isotope data. European Journal of Mineralogy 3, 415–428.

Civetta, L., Galati, R., Santacroce, R., 1991b. Magma mixing and convective compositional layering within the Vesuvius magma chamber. Bulletin of Volcanology 53, 287–300.

Civetta, L., Orsi, G., Pappalardo, L., Fisher, R.V., Heiken, G., Ort, M., 1997. Geochemical zoning, mingling, eruptive dynamics and depositional processes — the Campanian Ignimbrite, Campi Flegrei caldera, Italy. Journal of Volcanology and Geothermal Research 75, 183–219.

Clynne, M.A., 1999. A complex magma mixing origin for rocks erupted in 1915, Lassen Peak, California. Journal of Petrology 40 (1), 105–132.

Corrado, G., Guerra, I., Lo Bascio, A., Luongo, G., Rampoldi, F., 1977. Inflation and microearthquake activity of Phlegraean Fields, Italy. Bulletin Volcanologique 40 (3), 169–188.

Cortés, J.A., Wilson, M., Condliffe, E., Francalanci, L., Chertkoff, D.G., 2005. The evolution of the magmatic system of Stromboli volcano during the Vancori period (26–13.8 ka). Journal of Volcanology and Geothermal Research 147, 1–38.

Couch, S., Sparks, Carrol, M.R., 2001. Mineral disequilibrium in lavas explained by convective self-mixing in open magma chambers. Nature 411, 1037–1039.

D'Antonio, M., Civetta, L., Orsi, G., Pappalardo, L., Piochi, M., Carandente, A., de Vita, S., Di Vito, M.A., Isaia, R., Southon, J., 1999. The present state of the magmatic system of the Campi Flegrei caldera based on the reconstruction of its behavior in the past 12 ka. Journal of Volcanology and Geothermal Research 91, 247–268.

D'Antonio, M., Tonarini, S., Arienzo, I., Civetta, L., Di Renzo, V., 2007. Components and processes in the magma genesis of the Phlegrean Volcanic District (South Italy). Geological Society of America Special Paper, vol. 418, pp. 203–220.

de Vita, S., Orsi, G., Civetta, L., Carandente, A., D'Antonio, M., Di Cesare, T., Di Vito, M., Fisher, R.V., Isaia, R., Marotta, E., Ort, M., Pappalardo, L., Piochi, M., Southon, J., 1999. The Agnano–Monte Spina eruption (4.1 ka) in the resurgent, nested Campi Flegrei caldera (Italy). Journal of Volcanology and Geothermal Research 91, 269–301.

De Vivo, B., Rolandi, G., Gans, P.B., Calvert, A., Bohrson, W.A., Spera, F.J., Belkin, H.E., 2001. New constraints on the pyroclastic eruptive history of the Campanian volcanic Plain (Italy). Mineralogy and Petrology 73, 47–65.

Deino, A.L., Orsi, G., Piochi, M., de Vita, S., 2004. The age of the Neapolitan Yellow Tuff caldera-forming eruption (Campi Flegrei caldera — Italy) assessed by $^{40}Ar/^{39}Ar$ dating method. Journal of Volcanology and Geothermal Research 133, 157–170.

Di Filippo, G., Lirer, L., Maraffi, S., Capuano, M., 1991. L'eruzione di Astroni nell'attività recente dei Campi Flegrei. Bollettino della Società Geologica Italiana 110, 309–331 (Rome).

Di Girolamo, P., Ghiara, M.R., Lirer, L., Munno, R., Rolandi, G., Stanzione, D., 1984. Vulcanologia e petrologia dei Campi Flegrei. Bollettino della Società Geologica Italiana 103, 349–413 (Rome).

Di Renzo, V., Di Vito, M.A., Arienzo, I., Carandente, A., Civetta, L., D'Antonio, M., Giordano, F., Orsi, G., Tonarini, S., 2007. Magmatic history of Somma–Vesuvius on the basis of new geochemical and isotopic data from a deep borehole (Camaldoli della Torre). Journal of Petrology 48 (4), 753–784.

Di Vito, M.A., Lirer, L., Mastrolorenzo, G., Rolandi, G., 1987. The Monte Nuovo eruption (Campi Flegrei, Italy). Bulletin of Volcanology 49, 608–615.

Di Vito, M.A., Isaia, R., Orsi, G., Southon, J., de Vita, S., D'Antonio, M., Pappalardo, L., Piochi, M., 1999. Volcanism and deformation in the past 12 ka at the Campi Flegrei caldera (Italy). Journal of Volcanology and Geothermal Research 91, 221–246.

Elter, P., Grasso, M., Parotto, M., Mezzani, L., 2003. Structural setting of the Apennine–Maghrebian thrust belt. Episodes 26, 205–211.

Fedele, F.G., Giaccio, B., Isaia, R., Orsi, G., 2003. The Campanian Ignimbrite eruption, Heinrich Event 4, and Palaeolithic change in Europe: a high-resolution investigation. In: Robock, A., Oppenheimer, C. (Eds.), Volcanism and the Earth's Atmosphere, vol. 139. American Geophysical Union Geophysical Monograph Series, Washington, D.C., pp. 301–325.

Fisher, R.V., Orsi, G., Ort, M., Heiken, G., 1993. Mobility of large-volume pyroclastic flow — emplacement of the Campanian Ignimbrite, Italy. Journal of Volcanology and Geothermal Research 56, 205–220.

Folch, A., Martì, J., 1998. The generation of overpressure in felsic magma chambers by replenishment. Earth and Planetary Science Letters 163, 301–314.

Huppert, H.E., Sparks, R.S.J., Turner, J.S., 1982. Effects of volatiles on mixing in calc-alkaline magma systems. Nature 297, 554–557.

Isaia, R., D'Antonio, M., Dell'Erba, F., Di Vito, M.A., Orsi, G., 2004. The Astroni volcano: the only example of close eruptions within the same vent area in the recent history of the Campi Flegrei caldera (Italy). Journal of Volcanology and Geothermal Research 133, 171–192.

Kretz, R., 1983. Symbols for rock-forming minerals. American Mineralogist 68, 277–279.

Le Maitre, R.W., 1989. In: Bateman, P., Dudek, A., Keller, J., Lameyr, J., Le Bas, M.J., Sabine, P.J., Schmid, R., Sørensen, H., Streckeisen, A., Woolley, A.R., Zanettin, B. (Eds.), A Classification of Igneous Rocks and Glossary of Terms: Recommendations of the International Union of Geological Sciences Subcommission on the

Systematics of Igneous Rocks. Blackwell Scientific Publications, Trowbridge, Wilts, England, pp. 1–193.
Leeman, W.P., Sisson, V.B., 1996. Geochemistry of boron and its implications for crustal and mantle processes. In: Grew, E.S., Anovitz, L.M. (Eds.), Boron: Mineralogy, Petrology and Geochemistry. Reviews in Mineralogy, vol. 33. Mineralogical Society of America, Washington, D.C., pp. 645–708.
Leeman, W.P., Sisson, V.B., Reid, M.R., 1992. Boron geochemistry of the lower crust: evidence from granulite terranes and deep crustal xenoliths. Geochimica et Cosmochimica Acta 56, 775–788.
Murphy, M.D., Sparks, R.S.J., Barclay, J., Carrol, M.R., Brewer, T.S., 2000. Remobilization of andesite magma by intrusion of mafic magma at the Soufrière Hills volcano, Montserrat. West Indies. Journal of Petrology 41 (1), 21–42.
Nagakawa, M., Wada, K., Wood, C.P., 2002. Mixed magmas, mush chambers and eruption triggers: evidence from zoned clinopyroxene phenocrysts in andesitic scoria from the 1995 eruptions of Ruapehu volcano, New Zealand. Journal of Petrology 43 (12), 2279–2303.
Orsi, G., Gallo, G., Zanchi, A., 1991. Simple shearing block resurgence in caldera depressions. A model from Pantelleria and Ischia. Journal of Volcanology and Geothermal Research 47, 1–11.
Orsi, G., D'Antonio, M., de Vita, S., Gallo, G., 1992. The Neapolitan Yellow Tuff, a large-magnitude trachytic phreatoplinian eruption: eruptive dynamics, magma withdrawal and caldera collapse. Journal of Volcanology and Geothermal Research 53, 275–287.
Orsi, G., Civetta, L., D'Antonio, M., Di Girolamo, P., Piochi, M., 1995. Step-filling and development of a three-layers magma chamber: the Neapolitan Yellow Tuff case history. Journal of Volcanology and Geothermal Research 67, 291–312.
Orsi, G., de Vita, S., Di Vito, M.A., 1996. The restless, resurgent Campi Flegrei nested caldera (Italy): constraints on its evolution and configuration. Journal of Volcanology and Geothermal Research 74, 179–214.
Orsi, G., Civetta, L., Del Gaudio, C., de Vita, S., Di Vito, M.A., Isaia, R., Petrazzuoli, S., Ricciardi, G., Ricco, C., 1999a. Short-term ground deformations and seismicity in the nested Campi Flegrei caldera (Italy): an example of active block resurgence in a densely populated area. Journal of Volcanology and Geothermal Research 91, 415–451.
Orsi, G., Petrazzuoli, S., Wohletz, K., 1999b. The interplay of mechanical and thermo-fluid dynamical systems during an unrest episode in calderas: the Campi Flegrei caldera (Italy) case. Journal of Volcanology and Geothermal Research 91, 453–470.
Orsi, G., Di Vito, M.A., Isaia, R., 2004. Volcanic hazard assessment at the restless Campi Flegrei caldera. Bulletin of Volcanology 66, 514–530.
Ort, M., Orsi, G., Pappalardo, L., Fisher, R.V., 2003. Anisotropy of magnetic susceptibility studies of depositional processes in the Campanian Ignimbrite, Italy. Bulletin of Volcanology 65, 55–72.
Pabst, S., Wörner, G., Civetta, L., Tesoro, R., 2007. Magma chamber evolution prior to the Campanian Ignimbrite and Neapolitan Yellow Tuff eruptions (Campi Flegrei, Italy). Bulletin of Volcanology 70, 961–976.
Pappalardo, L., Civetta, L., D'Antonio, M., Deino, A., Di Vito, M., Orsi, G., Carandente, A., de Vita, S., Isaia, R., Piochi, M., 1999. Chemical and Sr — isotopical evolution of the Phlegraean magmatic system before the Campanian Ignimbrite (37 ka) and the Neapolitan Yellow Tuff (12 ka) eruptions. Journal of Volcanology and Geothermal Research 91, 141–166.
Pappalardo, L., Piochi, M., D'Antonio, M., Civetta, L., Petrini, R., 2002. Evidence for multiple stage magmatic evolution during the past 60 kyr at Campi Flegrei (Italy) deduced from Sr, Nd ans Pb isotope data. Journal of Petrology 43, 1415–1434.
Perini, G., Tepley III, F.J., Davidson, J.P., Conticelli, S., 2003. The origin of K-feldspar megacrysts hosted in alkaline potassic rocks from central Italy: a track for low-pressure processes in mafic magmas. Lithos 66, 223–240.
Perugini, D., Poli, G., Gatta, G.D., 2002. Analysis and simulation of magma mixing processes in 3D. Lithos 65, 313–330.
Petrelli, M., Perugini, D., Poli, G., 2006. Time-scales of hybridisation of magmatic enclaves in regular and chaotic flow fields: petrologic and volcanologic implications. Bulletin of Volcanology 68, 285–293.
Prelević, D., Foley, S.F., Cvetkovic, V., Romer, R.L., 2004. The analcime problem and its impact on the geochemistry of the ultrapotassic rocks from Serbia. Mineralogical Magazine 68, 633–648.
Putnis, C.V., Geisler, T., Schmid-Beurmann, P., Stephan, T., Giampaolo, C., 2007. An experimental study of the replacement of leucite by analcime. American Mineralogist 92, 19–26.
Ramos, F.C., Wolff, J.A., Tollstrup, D.L., 2005. Sr isotope disequilibrium in Columbia River flood basalts: Evidence for rapid shallow-level open-system processes. Geology 33 (6), 457–460.
Rosi, M., Sbrana, A., 1987. The Phlegraean Fields. Consiglio Nazionale delle Ricerche, Quaderni de "La Ricerca Scientifica", Rome, 114, pp. 1–175.
Santacroce, R., Bertagnini, A., Civetta, L., Landi, P., Sbrana, A., 1993. Eruptive dynamics and petrogenetic processes in a very shallow magma reservoir: the 1906 eruption of Vesuvius. Journal of Petrology 34, 383–425.
Sartori, R., 2003. The Tyrrhenian back-arc basin and subduction of the Ionian lithosphere. Episodes 26, 217–221.
Sparks, R.S.J., Sigurdsson, H., Wilson, L., 1977. Magma mixing: a mechanism for triggering acid explosive eruptions. Nature 267, 315–318.
Stormer, J.C., Nicholls, J., 1978. XLFRAC: a program for interacting testing of magmatic differentiation models. Computers and Geosciences 4, 143–159.
Streck, M.J., Grunder, A.L., 1999. Enrichment of basalt and mixing of dacite in the rootzone of a large rhyolite chamber: inclusions and pumices from the Rattlesnake Tuff, Oregon. Contributions to Mineralogy and Petrology 136, 193–212.
Suzuki, Y., Nakada, S., 2007. Remobilization of highly crystalline felsic magma by injection of mafic magma: constraints from the middle six century eruption at Haruna volcano, Honshu, Japan. Journal of Petrology 48 (8), 1543–1567.
Taylor, S.R., McLennan, S.M., 1985. The Continental Crust: its Composition and Evolution. Blackwell, Oxford, pp. 1–317.
Tonarini, S., Pennisi, M., Leeman, W.P., 1997. Precise boron isotopic analysis of complex silicate (rock) samples using alkali carbonate fusion and ion exchange separation. Chemical Geology 142, 129–137.
Tonarini, S., Pennisi, M., Adorni-Braccesi, A., Dini, A., Ferrara, G., Gonfiantini, R., Wiedenbeck, M., Gröning, M., 2003. Intercomparison of boron isotope and concentration measurements: Part I: Selection, preparation and homogeneity tests of the intercomparison materials. Geostandards Newsletter 27, 21–39.
Tonarini, S., Leeman, W.P., Civetta, L., D'Antonio, M., Ferrara, G., Necco, A., 2004. B/Nb and δ^{11}B systematics in the Phlegrean Volcanic District (PVD). Journal of Volcanology and Geothermal Research 133, 123–139.
Troll, V.R., Schmincke, H.-U., 2002. Magma mixing and crustal recycling recorded in ternary feldspar from compositionally zoned peralkaline ignimbrite "A", Gran Canaria, Canary Islands. Journal of Petrology 43 (2), 243–270.
Viccaro, M., Ferlito, C., Cortesogno, L., Cristofolini, R., Gaggero, L., 2006. Magma mixing during the 2001 event at Mount Etna (Italy): effects on the eruptive dynamics. Journal of Volcanology and Geothermal Research 149, 139–159.
Vogel, T.A., Ryerson, F.J., Noble, D.C., Younker, L.W., 1987. Limits to magma mixing based on chemistry and mineralogy of pumice fragments erupted from a chemically zoned magma body. Journal of Geology 95 (5), 659–670.
Weinberg, R.F., Leitch, A.M., 1998. Mingling in mafic magma chambers replenished by light felsic inputs: fluid dynamical experiments. Earth and Planetary Science Letters 157, 41–56.
Wohletz, K., Orsi, G., de Vita, S., 1995. Eruptive mechanisms of the Neapolitan Yellow Tuff interpreted from stratigraphic, chemical and granulometric data. Journal of Volcanology and Geothermal Research 67, 263–290.